UNIVERSITÀ DEGLI STUDI DI GENOVA

DEPARTMENT OF INTERNAL MEDICINE

CLINICAL AND EXPERIMENTAL IMMUNOLOGY SCHOOL

PhD THESIS

Development of an in vitro murine three-dimensional tumor model to study the micro-environment ability to tune cell's features

SUPERVISORS: CANDIDATE:
Prof. Gilberto Filaci   FRANCESCA COSTABILE
Prof. Maddalena Mastrogiacomo   Matr. S4452780

Foreword

This dissertation is an original intellectual product of the author, F. Costabile. When a student's research is done in collaboration with a big team, it easily turns into an ambitious and interdisciplinary work, that gives the student the tools to professionally grow through tutors' guidance and their praiseworthy experience.

Given the challenging attitude of the student, this work has been focused on an emerging research topic, such as the development of a tumor three dimensional model, able to add extremely important features to the current utilized in vitro methodology.

Even though the lack of large literature about the topic and the indispensable interdisciplinary knowledge needed during the progression of the work, the presented dissertation shows clear and rigorous results supporting the preset aim.

Although the student had to face data collection and analysis in different biological fields, she was able to establish a harmonious work that led to well-written dissertation.

Table of contents:

1. Introduction

1.1 Tumor microenvironment

The tumor microenvironment (TME) is a complex system, shaped by direct interactions among different cell types, soluble factors and between cells and the extracellular matrix (ECM)[1]. In this scenario cancer cells just represent one side of the TME, being located in the parenchyma of the abnormal tissue. The stroma of the tumor tissue is instead composed of mesenchymal cells supporting the structure (cancer associated fibroblasts, tumor associated macrophages), endothelial cells and pericytes providing *de novo* nourishing system, immune system cells responding to the cancer insult (T-cells, B-cells, Natural killer cells).

It is interesting to observe how structural cells behave so differently based on the environment they are challenged to. For example, in a normal tissue epithelial cells are meant to form the epithelium layer, which consists of epithelial cells associated by cell-to-cell junctions such as tight junctions, adherens junctions, desmosomes, and gap junctions. Epithelium layer is also polarized (apicobasal polarity) being attached to the basal lamina by ECM junctions. All these junctions provide immobility to the epithelium. After the beginning of the neoplastic process, the epithelial-mesenchymal transition (EMT) has been observed. EMT is a complex course where epithelial cells are transformed into mesenchymal cells. Concisely, epithelial cells lose core properties including the apicobasal polarity, cell adhesion, and increase mesenchymal cell properties during the transition[2,3]. Mesenchymal cells, like fibroblasts, do not have these features and only have focal points that adhere to their neighbor mesenchymal cells. They do not have junctions for basal lamina. After the beginning of the neoplastic process, fibroblasts are called "cancer-associated fibroblasts" (CAF). They constitute 5–10% of the total cells of many solid epithelial tumors, such as pancreas, stomach, and breast cancers[4]. CAFs are a key component of the tumour microenvironment with diverse functions, including matrix deposition and remodelling, extensive reciprocal signalling interactions with cancer cells and crosstalk with infiltrating leukocytes[5]. In addition, they are particularly effective in carcinogenesis, tumor progression, and metastasis[6,7]. Therefore, epithelial cells may acquire several abilities such as motility, invasion, and malignant features via EMT[8]. EMT is a naturally occurring trans differentiation process and is critical during embryonic development and organogenesis (type-1 EMT - physiologic EMT). This phenomenon also occurs during wound healing, tissue regeneration, organ fibrosis (type-2 EMT), and carcinogenesis (type-3 EMT, known as the "oncogenic epithelial-mesenchymal transition"). However, it is still unclear how noncancerous cells and noncellular components of the tumor niche collaborate and assist cancer cells to acquire invasive and metastatic features. Recently, the genetic and biochemical properties that underlie acquirement of cancer cell invasiveness and metastasis are the major areas of intensive research. In addition, Yang et al. reported that tumor cells were able to behave like mesenchymal cells and express mesenchymal markers[9]. However, the specific signals that are induced during the pathologic EMT in epithelial cancers remain unclear[10].

In the tumor microenvironment, a unique network has been shown to be created by mainly carcinoma-associated fibroblasts and cancer stem cells (CSCs) with the participant of other noncancerous cells. This network modulates and regulates different mechanisms of the

neoplastic processes, such as carcinogenesis, tumor progression, angiogenesis, and metastasis[11]. CSCs share similar properties with normal stem cells, including the ability to self-renew, making up the bulk of the tumour[12]. Under normal physiological condition, normal stem cells usually reside in a quiescent state which is maintained by a specialised niche. Only upon receipt of a stimulating signal, the stem cells become activated to divide and proliferate. Any genetic mutation causing stem cells to become independent of growth signals, or to resist antigrowth signals, will cause the stem cells to undergo uncontrolled proliferation and possible tumorigenesis[13]. CSCs therefore play an active role throughout the cancer progression as well as in therapy resistance by manipulating their adaptation, favouring their growth and survival. Therefore, better understanding of CSCs behaviours, which differs according to their microenvironment corresponding to the different stages of cancer, is important to help design more effective therapeutic strategy targeting these populations.

Tumour progression involves complex cellular and molecular processes. Conceptually, carcinogenesis can be divided into the following stages: initiation, promotion, and progression, and these stages are concomitant with complex and dynamic cellular events[14]. Therefore, carcinogenesis often initiates with cells losing their growth control due to accumulated mutations, leading to uncontrolled proliferation[15]. With no therapeutic intervention, the cancer becomes increasingly progressive, facilitated by the surrounding tumour microenvironment providing tumour growth supportive signals. The cancer no longer remains localised but begins searching for new soil to compensate increasing needs to survive, via metastatic cascade. In this milieu, research has suggested that cancer cells are capable of influencing their surrounding tumour microenvironment to make it permissive for them to survive and evolve with more resistant and aggressive phenotypes as the cancer progresses[12]. Central to all cancers is inflammation, phenomenon presents during caner initiation, but also persisting during its growth, playing a central role during progression, invasion, angiogenesis, and metastasis[16,17]. To link the possible roles of inflammation and CSC in the cancer initiation, evidence can be drawn from the changes in the microenvironment within the stem cell niche. It has been observed that the formation of CSCs is preceded by the transition of the stem cell niche into an area of high concentrations of reactive oxygen species (ROS) and reactive nitrogen species (RNS), lipid peroxidation products (LPPs), inflammatory cytokines and chemokines[18]. Prolonged exposure of these stem cells' DNA to assaults by ROS/RNS and LPPs can produce varying degrees of genetic mutations that over time is beyond repair, and these cumulatively may drive the conversion a stem cell into a cancer stem cell[19].

As the tumour develops, it becomes increasingly important for the cancer cells to sustain their growth and functions achieved through formation of tumour microenvironment by recruiting cellular components and modulating their extracellular matrix (ECM). Additionally, the tumour mass is increasingly hypoxic due to increase in tumour size, causing the formation of new vasculatures to facilitate diffusion of nutrients and oxygen to the cancer cells through angiogenesis process[20,21]. Thus, the niche plays key roles in CSCs promotion and maintenance by regulating their stemness properties via activation of key signalling pathways involved in the self-renewal, angiogenesis and promotes the long-term survival of CSC. CSCs however, do not play the passive roles of receiving end but they work together in modulating the niche in their favour, predominantly through their interactions with the components in the niche. Cancer cells and CSCs "educate" the surrounding cells, such as the stromal and immune cells,

by secreting signals that recruit, transform and alter the functions and activities of the micro environment which in turn facilitate growth and progression of tumour[22].

Cancer promotion stage may be considered as completed when an abnormal group of cells are irreversibly committed to eventual development of malignant characteristics and to indefinite multiplication[23]. The time between the end of promotion and the emergence of a recognisable malignant tumour is called progression. During progression, the pathological cells expands many times and, importantly, they escape apoptosis[24]. Their morphology definitely changes with gross shape and polarity loss, they show internal changes to organelles such as the nucleus (nuclear enlargement and increased nuclear-to-cytoplasmic ratio, nuclear membrane irregularities), the cytoplasm is scarce and intensely colored or, on the contrary, is pale. Noteworthy, changes in the nucleus morphology imply development of chromosomal defects of various kinds (hyperchromasia, and abnormal chromatin distribution) and abnormal mitotic at cell division[25]. Nuclear changes explain the presence of different cell clones and genetic anomalies associated with these changes[26]. The phenotypic heterogeneity improves the cellular response to environmental challenges during tumorigenesis and enhances the rate of evolutionary changes[27]. In order to sustain the mitosis high rate, extensive changes arise at chemical level in the sugar sequences of cancer cells. Abnormal glycolysis processes occur in mitochondrial membranes, known in the literature as the "Warburg phenomenon". Due to their abnormal mitosis rate, cancer cells choose glycolysis compared to oxidative phosphorylation (OXPHOS). Although the energetic yield per molecule of glucose is much lower for aerobic glycolysis compared to OXPHOS, when glucose is in excess and flux through the pathway, glycolysis has the potential to produce ATP at a faster rate[28].

Also, the cell membrane plays an extremely important role in the malignant transformation: cell surface receptors can increase or decrease in number, eventually changing the signal transduction and cells sensitivity to their environment; new surface molecules, characteristic of the embryonic tissue, can be present on the surface of cancer cell, leading to abnormal behaviour[29]. Specialised cell to cell junctions are lost and, gradually, the extracellular matrix is modified by increased destruction, by aberrant replacement, or by both[30,31]. Tumour and stromal cells express increased levels of ECM-degrading proteases that have multiple functions during tumour progression. First, proteolytic degradation of ECM components allows progressive destruction of the normal ECM and its replacement with tumour-derived ECM. Second, ECM degradation is an important driver of cancer cell motility. Third, ECM-binding of soluble signalling molecules such as growth factors makes them insoluble and inactive and action of proteases liberate them. The enhanced protease activity in tumours causes subsequent ECM degradation that releases the ECM-bound growth factors and thereby increases their bioavailability. Last, the cleavage of long ECM components produces bioactive, shorter fragments with distinct functions that can be pro- or anti-tumourigenic compared to the full-length ECM component. These fragments often contain structures similar to chemokines or cytokines and are therefore termed matrikines. Matrikines play an important role in angiogenesis and neo-tumor vasculature[32]. Thus, tissues are dynamically shaped by bidirectional communication between resident cells and the ECM through cell-matrix interactions and ECM remodelling. Tumours, therefore, leverage ECM remodelling to create a microenvironment that promotes tumourigenesis and metastasis. All these findings suggest that a better understanding of tumourigenic ECM remodelling would be crucial not just for new

biological mechanisms' discovery, but, more important, for new target discovery and development of new therapeutic treatments for cancer patients. Hence, the necessity of create a specific research field of research focus on TME, inclusive of different kind of cells and ECM.

1.2 Three-dimensional tumor models

Given the emerging importance of the TME modulating cells' morphology and function, more sophisticated tumor models, incorporating TME features, are needed to elucidate cellular, molecular, and immunologic mechanisms of tumor response and resistance [33,34]. An intensive investigation of *in vitro* models able to study tumor complexity has led to the generation of different three-dimensional (3D) culture methods that better mimic *in vivo* conditions compared to the usual 2D culture methods [35,36].

The 3D mono- and co-cultures are able to reproduce some "*in vivo* features" such as 3D cell morphology, which permits cells to better execute their function and enables them to deposit significant increased amount of ECM [37,38]. Furthermore these culture techniques also induce cellular phenotype switch from physiologic to pathologic profile related to EMT and CAF markers [39–42].

Recent study on cancer 3D models have been focused on cultivation of cells as a "single cell" or as a spheroid group of cells, with or without different types of matrices [33–35].

When cell lines have the ability to self-assemble, one 3D culturing method possible is to produce spheroids. There are several systems for culturing cells in spheroids, e.g., hanging drop, on scaffolds and on hydrogels, and these cultures have their applications in drug and nanoparticles testing, and disease modelling [43]. In this work we utilized the hanging drop system to generate spheroids made of one or two cell lines.

Spheroids are cell aggregates, self-assembling in an environment that prevents attachment to a flat surface. Spheroid formulation is possible because of membrane proteins (integrins) and extracellular matrix proteins. Hanging drop is one method of obtaining scaffold-free cell cultures. This method does not require specialized equipment but just involves small volumes of cell suspension (usually 20 µL). The cell suspension can be placed into the well of a special plate, which is turned upside down so that the cell suspension becomes a hanging drop held by surface tension. Cells remain in direct contact with each other and with the ECM. However, also without any special plate, the simplest way to obtain cell culture in hanging drop is to put a drop with a cell suspension onto the inside of a lid of a culture plate. After reversing, microgravity concentrates cells at the bottom of the drop. The hanging drop method can be used also to co-culture several cell lines. Unfortunately, oxygen supply to spheroid culture is a very important factor limiting cell viability during culturing cells. Indeed, this 3D culture method can be a suitable culture system until indicatively 20 days. This 3D culture system is perfect to study the initial stage of the tumor microenvironment, to understanding the biological mechanisms, different pathways, cells cross-talk and morphology changing of the different of cells present in the tumor bulk. Moreover, this is a scaffold-free 3D system, allowing to appreciate the ECM deposit by the cells forming the spheroid. If the cell line does not produce ECM, the spheroid has low chance to develop.

In order to study the advanced tumor stage mechanisms, different 3D systems are required to overstep the limitation of the spheroid system. Different types of matrices have been developed to be utilized as scaffold for cell cultures. In order to induce cell adhesion, proliferation, and activation, materials used for the fabrication of scaffolds must possess requirements such as intrinsic biocompatibility and proper chemistry to induce molecular biorecognition from cells. Scaffold should host cell adhesion, proliferation, and ECM production: in conclusion, the scaffold should surrogate the missing ECM. Most scaffolds are produced from natural or synthetic polymer [44]. Naturally derived polymer materials, such as collagen or fibroin, generally exhibit good biocompatibility and low toxicity[36,39,45]. However, batch-to-batch variability and difficult processing does occur for some polymers, which can be considered a drawback. Indeed, a valid alternative to the natural matrices are the synthetic degradable polymers, often used as scaffold materials thanks to their high versatility, properties, reproducibility, and good workability. The most used degradable polymers as scaffold materials are polyglycolic acid (PGA), polylactic acid (PLA), polycaprolactone (PCL) and polyurethanes. In contrast, synthetic polymers are generally less biocompatible than the natural ones [44].

1.3 Decellularization technique

However, in 3D cell cultures the biological cross talk between cells and the scaffold is controlled by the material properties and scaffold characteristics. Even if these scaffolds allow cell adhesion and proliferation, unfortunately they do not faithfully represent the *in vivo* extracellular matrix: the grand variety of proteins and glycosaminoglycans, especially in the tumor microenvironment, are exclusive of the original tissue *in vivo* and they cannot be present in these scaffolds [46–49]. Among the new applications in cancer biotechnology, a convincing alternative method able to overstep the poor variety of proteins and glycosaminoglycans, is the *in vitro* application of tumor tissue derived ECM matrices. These matrices are obtained from fresh tumor spacemen processed by decellularization technique, that provides a cell-free scaffold avoiding the loss of the physics and biological original features [50,51]. Many methods have been examined to perform decellularization [52]. The most popular decellularization technique combine chemical, biological and physical approaches, including multiple washings usually with surfactants and hypertonic solutions, and enzymatic DNA digestion during agitations [53–60]. Basically, the chemical decellularization methods function by immersing the tissue in a solution containing an acid, alkaline base, alcohol, chelating agent, or detergents, that destroy cellular and nuclear components and induce cellular lysis. Chelating agents like Ethylenediaminetetraacetic acid (EDTA) are used with enzymes or detergents to improve cell nuclei removal. EDTA application promotes cell detachment by reducing cell-matrix and cell-cell adhesion through the chelation of extracellular Ca2+ ions that are necessary for the activation of Ca2+ dependent cell adhesion molecules such as integrins and cadherins. Detergents such as sodium deoxycholate (SD), sodium dodecyl sulfate (SDS), Triton X-100 and N-Lauroylsarcosine are used to lyse cell membrane, to solubilize membrane proteins and lipids and also to remove cytosolic and genomic material. Enzymatic methods are mainly based on the use of nucleases (DNase and RNase) to digest nucleic acids. Decellularization protocols also often include a physical decellularization step such as mechanical agitation or freeze/thaw

cycles[61]. Therefore, the combination of chemical, biological and physical mechanisms used togheter allow a successful decellularization. After the treatment, the ECM is depleted from its native cells and genetic materials (such as DNA and RNA found in the nucleus, mitochondria, and cytoplasm). The ECM, that ideally retains its indispensable structural, biochemical and biomechanical cues, can then be recellularized to produce a functional tissue or organ. In order to assess the decellularization success, the easiest method is a histochemical analysis of the tissue, showing complete absence of cellular and nuclear components while the extracellular matrix remained intact. The most common staining is the trichrome staining. The word trichrome means "three colours": the first staining protocol that was described as "trichrome" was Mallory's trichrome stain, which differentially stained erythrocytes to a red colour, muscle tissue to a red colour, and collagen to a blue colour. Some other trichrome staining protocols are the Masson's trichrome stain, Lillie's trichrome, and the Gömöri trichrome stain, really similar to each other except for the derivation of the dyes.

Tissue engineering and 3D *in vitro* cultures are complex procedures, which includes processes of decellularization, described above, and recellularization by active cells. Recellularization process requires appropriate cell sources, an optimal seeding method, and a physiologically relevant culture method[62]. For example, coating of tissue derived matrices has been employed as a technique to enhance cell seeding. Matrigel, collagen, fibrinogen and thrombin are some of the materials utilized for coating and enhance cells attachment to the 3D scaffold. These materials help to create an external structure out of the tissue, that will not allow cells to disperse around in the plate or other artificial environment where the culture is performed. Moreover, optimal cell density and cell number will need to be determined for seeding. Increasing the cell density does not increase the possibility of recellularization. Indeed, the tissue can allow the colonization of a certain number of cells: after that amount, the remaining cells will be not able to colonize, but they will just consume the nutrients and provoke less fitness of the cells that are actually colonising the tissue. Also, the derivation of cells might impact the recellularization success. Of course, an immortalized cell line and cells belonging to the stroma like mesenchymal cells, endothelial cells and pericytes, will have many more chances to colonize the tissue compared to cells with less duplication rate and with special nutrition and environment requirements.

Due to these complications, some decellularized tissues have limited potential for recellularization. To overcome this problem decellularized tissues are often transformed into hydrogels. Over 70 papers describe the use of ECM-derived hydrogels from a wide variety of organs [63]. First publications in cancer field highlighting the advantages of tumor derived ECM 3D hydrogel came out just few years ago. For example, the study of Romero-López et al. 2017 is executed with hydrogel matrices and shows the impact of ECM on cell metabolism: cells cultivated on tumor derived ECM hydrogel produce higher levels of free NADH compare to the same cells cultivated on scaffolds generated from different ECM: high levels of free NADH is a characteristic of cancer environment due to a higher cell glycolysis rate [28]. Moreover, the same study shows how endothelial cells on tumor derived ECM hydrogel can reorganize in a very similar manner to *in vivo* scenario compared to endothelial cells seeded on not tumor derived ECM hydrogel. Without the hydrogel aid, experiment like cells migration and orientation would be challenging, due to the lacking cell penetration that is often observed with decellularized matrices.

In this work, we were looking for a model allowing us the study the microenvironment of a tumor in an advanced stage, since this is not possible with the creation of the spheroids. Therefore, we examinate the potential of a decellularization murine tumor as a 3D scaffold. We show the decellularization of the tissue and we examinate the matrix derived from the process. We also analyse the recellularization potential of that specific tissue and all the potential limits of the culture method. Overall, this study will help the cancer research community to understand more about the tumor extracellular matrix and the *in vitro* experimentation techniques able to incorporate this feature. Furthermore, here we describe a new method providing the matrix collapse measurement, using decellularized murine lung tissue and ImageJ software analysis. This analysis could help the researcher who is testing new physical, chemical or biological protocol for decellularization and will help to understand the consequences of the process on the spacemen avoiding its loss.

Importantly, 3D models incorporating ECM will allow the study of the tumor evading immune response mediated by the microenvironment. The ECM of malignant tumours is characterised as disorganized with increased production of some components compared to normal tissues. Whilst significant progress has been made in targeting aspects of the tumour microenvironment such as tumour immunity and angiogenesis, there are no therapies that address the cancer ECM. Importantly, immune function relies heavily on the structure, physics and composition of the ECM, indicating that cancer ECM and immunity are mechanistically inseparable. The simplest explanation for this is that ECM density provides a physical barrier, preventing interaction between immune effector and tumour cells. Although this may be contributory, the ECM was also reported to regulate immune cell motility, myeloid polarization, T-cell phenotype, immune cell metabolism and survival. To fully harness the potential of immunotherapy, treatments must be developed that address the functional contribution of the cancer ECM to tumour immunity (Fig. 1.1) [64]. The compositional and structural complexity of the ECM as well as significant intra-tumoural heterogeneity are still yet to be fully understood. Technological advances such as, indeed, tissue decellularization techniques and mass-spectrometry are beginning to address these issues. Going forward, it will be important to understand the specific contributions that individual ECM proteins make to matrix function as well as the signalling mechanisms regulating their deposition. Through this process, ECM modulation is likely to emerge as a fundamental cancer therapeutic. Therefore, a cunning *in vitro* model, including perhaps the tumor ECM of the specific patient, will be able to predict the outcome of different chemo/immunotherapeutic treatments, and will eventually drive the physician to an efficient and personalized drug therapy.
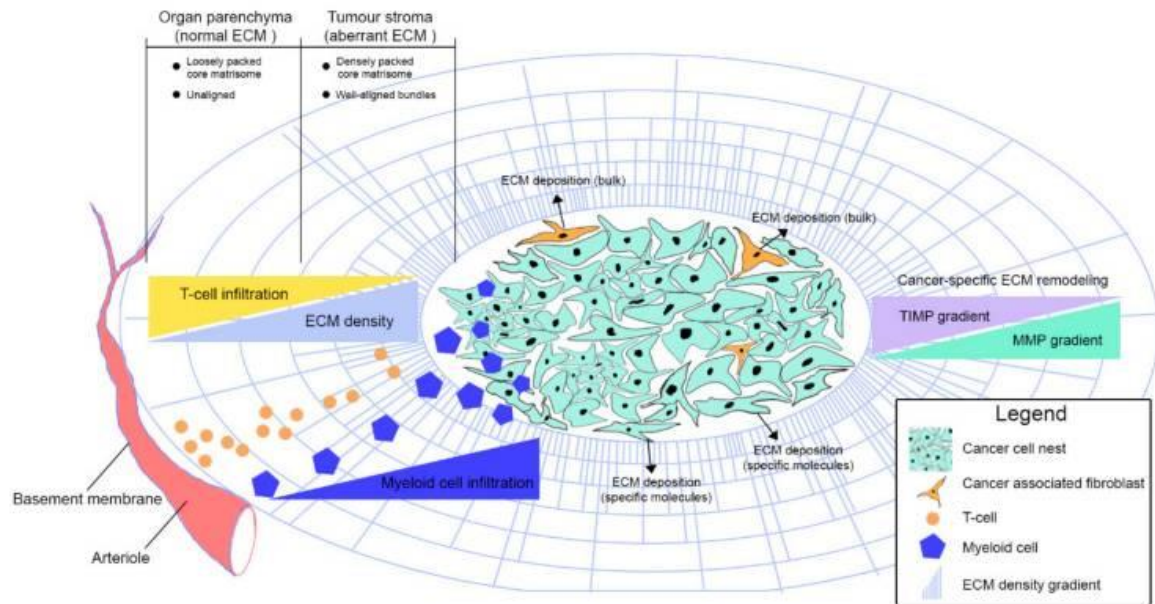
Fig. 1.1. Deregulation of ECM homeostasis in cancer affects immune infiltration. Schematic plan illustrating how growing solid tumours form cancer cell nests to educate tissue-resident fibroblasts that acquire a highly synthetic phenotype leading to the production of densely packed structural ECM components. Cancer cells partially contribute to ECM overproduction by secreting certain laminin chains as well as ECM regulators. The mechanisms underlying ECM remodelling in cancer are complex, with the general line being the subtle balance between ECM-decomposing enzymes (mainly MMPs) and their corresponding inhibitors (mainly TIMPs). One of the major consequences of ECM remodelling in cancer is collagen alignment, which partially regulates immune cell trafficking within the tumour microenvironment. Through this and other mechanisms, the cancer ECM excludes some immune cell subsets (such as infiltrating CD8+ T cells) whilst enabling active infiltration of others, such as macrophages and neutrophils. ECM extracellular matrix.[64]

2. Aim

Aim of this study is the development of an accurate *in vitro* 3D tumor model to study the impact of tumor ECM on the cells of the microenvironment. The understanding of the specific contributions that ECM proteins make to the tumor microenvironment became crucial due to the emergency of find alternative cures to the many cancer harbouring patients resistant to the existing therapies. The proposed study will provide a more realistic *in vitro* model that includes the ECM: this system will show if and how cells' behaviour is influenced by the tumor environment signals. Eventually, it will be a more precise model for *in vitro* drugs screening since the resistance of several therapies is known to be due to the ECM. Not less important, the model would be able to provide a partial substitution of *in vivo* experiment since the drug screening *in vitro* would be more efficient and restrictive.

Our experimental approach can be divided in two main experimental plans:

- the development of tumor spheroid model, helpful to understand the beginning stage of the nascent tumor;
- the development of a scaffold obtained by murine tumor tissue decellularization, utilized for the study of the advanced tumor stage, with a more complex ECM compared to the spheroid model.

The development of the spheroid helps to test the ability of a cell line to create a bulk since the system allow the growth in any directions. The addition of a second cell line in the spheroid is the first 3D model that helps to understand how the interaction between two different cell types can impact the tumor growth. The spheroid model is suitable for many studies, like the study of cell 3D morphology with the simple microscope observation, the study of ECM deposit with cytochemistry staining, the study of cell signaling with RNAseq or the research of specific molecules in the spheroid supernatant with ELISA assay. The limit of the spheroid model is the time, since, to date, the system does not provide oxygen import, necessary for the tumor bulk growth.

To create a 3D model able to allow the study of an advanced stage, we decided to create a scaffold from a mouse melanoma tumor, which is a material usually available in a research laboratory. Murine B16f10 derived tumors were processed for decellularization and studied to verify the efficacy as a natural scaffold for 3D culture system. The decellularization process let the tumor tissue maintain the biological properties of the ECM but at the same time is able to remove all the cells from the tissue, creating a suitable scaffold for 3D cell culture.

The decellularization process helps to support the idea of a human 3D culture system personalized for each patient affected by neoplasia. The ideal 3D model, indeed, would be made by tissues derived from the patient tumor biopsy, which will allow to test *in vitro* different chemo/immunotherapeutic treatments on the specific patient tissue before the administration of the drugs to the actual patient.

For all these reasons, we see an emergency to increase the study on new *in vitro* model, and especially 3D model that mimic as much as possible the tumor microenvironment. Advanced culture systems will be the tool allowing for the first-time an *in vitro* drug testing specific for each patient. The results will eventually drive the physician to a patient-personalized drug therapy.

3. Materials & Methods

Cell lines and animals. *B16F10* (ATCC® CRL-6475™) mouse skin melanoma cell line was cultivated in RPMI medium completed with 10% fetal calf serum (FCS), 1% penn/strep/fungizone (p/s/f) solution. *NIH/3T3* mouse fibroblast cell line (purchased from *Banca cellule* Interlab Cell Line Collection ICLC - IRCCS Azienda Ospedaliera Universitaria *San Martino* - IST Istituto Nazionale per la Ricerca sul Cancro) was cultivated in completed DMEM medium with 10% FCS, 1% p/s/f solution. C57/Black6 (BL/6) mice strain (purchased from Charles River) were used during this study.

Spheroids generation. *B16F10* murine melanoma cells were seeded alone or together with *NIH/3T3* mouse fibroblast cell line in a ratio 1:4 respectively, due to the different proliferation rate (700 B16F10 and 3000 NIH/3T3 cells) in 20 μL of DMEM completed medium under the lid of a sterile Petri dish[65]. Starting from day 5 of culture, medium was changed when needed.

Spheroids morphological analysis. At day 7, 3D morphology of spheroids generated by single cell line or by the co-culture of *B16F10* and *NIH/3T3* cells was observed by FV500 laser scanning confocal microscope and the classification of Kenny *et al.* 2007 was used to characterize cells organization in the bulk [66]. Spheroids' roundness level was measured with the roundness function for each spheroid using ImageJ software (Rasband, W.S., ImageJ, National Institutes of Health, Bethesda, MD, USA, http://rsb.info. nih.gov/ij/, 1997–2007).

Fluorescent Spheroids generation. *700 B16F10* cells stained with PKH26 dye (2 μM for each 10^6 cells) and 3000 *NIH/3T3* cells stained with CFSE (10 μM for each 10^6 cells) were seeded together in 20 μL of DMEM completed medium under the lid of a sterile Petri dish. The efficacy of the staining was evaluated with BD LSRFFortessa flow cytometer. Starting from day 5 of culture, medium was changed when needed. At day 7, spheroids were observed by FV500 laser scanning confocal microscope.

Animal procedures. Mice were handled in agreement with guidelines conforming to the Italian current regulations regarding the protection of animals used for scientific purposes. Procedures were specifically approved by the Ethical Committee for animal experimentation (CSEA) of the National Institute of Cancer Research and by the Italian Ministry of Health. 500000 *B16F10* mycoplasma free cells have been subcutaneously injected with 100 μL of Phosphate-buffered saline (PBS) in both flanks of 1 year old C57BL/6 female mice [33]. Mice have been sacrificed as the tumor reached 1 cm³ of volume following the formula [67]:

$$Tumor\ volume = 1/2(length \times width^2)$$

Sorting of GFP B16F10 Linterna™ cell line. Linterna™-B16-F10 Cell line, with turboGFP fluorescent protein in the cytoplasm (Innoprot, Derio, Spain), were utilized to generate spheroids with B16F10 and Red Fluorescent NIH/3T3 (Innoprot, Derio, Spain), 2D coculture of B16F10 and NIH/3T3, and a monolayer of B16F10. The GFP positive cells were isolated from the cultures by sorter FACS ARIA IIU-2. Dead cells were excluded by 7-Aminoactinomycin D (7AAD) staining.

RNA isolation and sequencing. Total RNA was extracted using Trizol reagent (Invitrogen, Carlsbad, CA) and the RNeasy kit (Qiagen, Hilden, Germany) according to the manufacturer's instructions. Total RNA concentration and quality were evaluated for inclusion in subsequent in vitro transcription assays based on a spectrophotometric absorption ratio of 260/280 >1.8 (NanoDrop, Wilmington, DE) and an RIN (RNA integrity number) value of >8.0 via electrophoretic analysis (Genewiz, NJ, USA). RNA was used for New Generation Sequencing library generation (Genewiz, NJ, USA). Differential Expression Analysis was made using NOIseq[68] and GFold[69].

Pathways analysis. The heatmap on the comparison between Mouse tumor in vivo vs Control; Spheroid vs Control; Coculture vs Control conditions was generated using R (a statistical and graphical software) and the heatmap.2 tool from the gplots package (version 3.1.1). The average normalized expression of the B16 Control condition between each of the three comparisons was used in generating the heatmap because NOISeq (a package in R that was used for Differential Expression Analysis; version 2.34.0) simulates the technical replicates in order to do the Differential Expression Analysis when there are not enough replicates available, hence each comparison yields a slightly different result.
DAVID (Database for Annotation, Visualization and Integrated Discovery) is a web-based tool for annotating genes by which it interprets biological meaning. DAVID KEGG pathway analysis was done using a list of 693 nonregulated genes that overlap between the mouse tumor *in vivo* vs spheroid condition.

Tumor derived cells recovering. Single cells suspension from murine tumor was obtained using 70 µm strainer. Cell suspension was washed with completed DMEM medium and used for recellularization experiments.

Tissue decellularization process. As soon as the tumor tissue was recovered it was kept in PBS 1% p/s/f solution and then sectioned in piece of approximately 3x3x1 mm. The whole decellularization process was done in sterile conditions: tumor pieces were washed in PBS 1% (p/s/f) and then processed for decellularization with 3 cycles of the following protocol: first solution consisted of 50 mM Tris-HCl pH 7.2, 5 mM MgCl$_2$, 0.01% (w:v) N-lauryl sarcosinate, endonuclease Benzonase (EDM Millipore, 101697) 41.8 Units/ml and 0.4 mM phenylmethylsulfonyl fluoride (16-20 hours); second hypertonic solution of 0.5 M KCl in sterile ultra-pure water (24-48 hours); third solution of ultra-pure water buffered 50 mM Tris-HCl pH 7.2 (4 hours) (Table 1.) (Wolfinbarger, Jr. et al. 2004). After the cycles, matrices were washed in sterile ultra-pure water for 72 hours and rinsed with PBS 1% Antibiotic-Antimycotic for at least 2 days. All the steps were performed at 25-30 °C with gentle shaking of 70-100 rpm and with sterile solutions in tissue culture hood. Samples were utilized or kept at – 80°C.

Immunohistochemistry and Immunofluorescence. Tissue OCT embedded were sectioned in 7 µm thick sections (if not differently specified) with a Leica CM3050S cryostat (Leica, Wetzlar, Germany) and stained for trichrome staining (Mallory trichrome, Bio Optica, Milan, Italy, 04-020802) or haematoxylin and eosin (H&E, Bio Optica, Mian, Italy, 04-065010). All the stainings were performed according to the manufacturer's instructions. For immunofluorescence (IF) analysis, the sections were blocked with 20% goat serum and

incubated with the primary antibody collagen VI (1:100, ab6588, Abcam, Cambridge, UK). Slides were then washed and incubated with the labelled Alexa Fluor 594 goat anti-rabbit IgG (H+L) (Invitrogen, A11007) diluted 1:400 or Alexa Fluor 488 goat anti-rabbit IgG (H+L) (Invitrogen, A11006) diluted 1:800. Finally, nuclei were stained with DAPI 500 ng/mL (Sigma-Aldrich, d9542). For each specimen, random pictures were collected with a direct microscope.

Scaffold recellularization. Tumor decellularized matrices or Polyurethane pieces were incubated overnight with 1 mL of growth medium containing 1% p/s/f at 4 °C. The day of the recellularization matrices were incubated at 37 °C in humidified incubator for at least 1 hour and then 300.000 cells were added. The matrices and cells were incubated at room temperature for 3 hours on the shaker. Then the medium was recovered and all the cells from the medium were resuspended in 6µL of fibrinogen. Matrices were placed on 24 well plate and fibrinogen with cells was added to them with 6µL of thrombin. Plate was kept for 30 minutes in humidified incubator at 37 °C and then 2 mL of growth medium was added. The matrices were moved in another well the day after and medium was replaced. After 7 of 15 days recellularized samples were fixed in 3.7% paraformaldehyde (PFA) + 2% sucrose and then included in a mix of OCT (optimal cutting temperature compound) and 20% Sucrose in a 1:1 ratio.

Matrix density measurement. Matrix density in fresh or decellularized 20 µm tissue sections, previously stained with DAPI and collagen type VI, deconvoluted and acquired with an Axio Imager A2M microscope equipped with an apotome module (Carl Zeiss, Jena, Germany), was measured with the Integrated density function for each z plan using ImageJ software (Rasband, W.S., ImageJ, National Institutes of Health, Bethesda, MD, USA, http://rsb.info. nih.gov/ij/, 1997–2007).

Scanning Electron Microscopy analysis (SEM). Fresh and decellularized tissues were sliced into segments of approximately 1 cm and fixed with 3% glutaraldehyde in 0.1 M phosphate buffer for 30 minutes. After fixation and 2 PBS washes of 30 seconds, the samples were dehydrated in a graded ethanol-water series from 15% to 100% ethanol, critical point dried using CO_2, and mounted on aluminium stubs. Samples were mounted and coated with a thin layer of carbon (approximately 20nm thick) using a K950X, Emitech carbon turbo evaporator. Images were recorded with a Tescan Vega 3 LMU SEM.

Matrix collapse measurement. Matrix collapse in fresh or decellularized murine lung tissue, previously dried using CO_2, coated with a thin layer of carbon and analysed with a Tescan Vega 3 LMU SEM, was measured comparing the mean of the area measurements of at least 6 alveoli for each sample using ImageJ software (National Institutes of Health, Bethesda, MD, USA, http://rsb.info. nih.gov/ij/, 1997–2007).

Statistical analysis. All graphs were performed using the GraphPad Prims Software 8. Data were reported as mean ± standard deviation. For the comparison of coupled experimental groups, the two-sided Student's *t*-test was used. A *p*-value < 0.05 was considered statistically significant (* *p*-value < 0.05; ** *p*-value < 0.01; *** *p*-value < 0.001).

First solution	
Compound	**Concentration**
mM Tris-HCl pH 7.2	50 mM
MgCl$_2$,	5 mM
N-lauryl sarcosinate	0.01%
endonuclease Benzonase	41.8 Units/ml
phenylmethylsulfonyl fluoride	0.4 mM

Second solution	
Compound	**Concentration**
KCl	0.5 M

Third solution	
Compound	**Concentration**
Tris-HCl pH 7.2	50 mM

Table 1. Solution for the decellularization process. Tumor samples were treated for 3 cycles with the described solutions, then washed in sterile ultra-pure water for 72 hours and rinsed with PBS 1% Antibiotic-Antimycotic for at least 2 days.

4. Results

Fibroblasts are needed for the generation of an early tumor stage 3D model

To establish a 3D model of an early tumor stage, we generated *B16F10* murine melanoma spheroids with the hanging drop culture system (Fig. 4.1). Interestingly, we found that these spheroids don't last more than one week. To keep the system lasting for longer, we generated spheroids made by *B16F10* and *NIH/3T3* fibroblast cell lines. At day 7, 14 and 21 of spheroids culture we evaluated ECM deposition through immunofluorescence (IF) analysis of collagen type VI on spheroids frozen sections (Fig. 4.2). The signal from collagen type VI is barely detectable when the spheroid is made just from *B16F10* cell line (Fig 4.1.A). Instead, the spheroid made by the co-culture of fibroblasts and tumor cells shows a clear collagen type VI signal (Fig. 4.1.B/C). However, Dapi signal (nuclei) decreases during the time (Fig. 4.1.C-D).

During the experiments we noticed differences in morphology among the different kind of spheroids: we decide to take a closer look to them using the confocal microscope. According to the 3D morphology classification of Kenny et al. 2007, *B16F10 + NIH/3T3* derived spheroids that we generated belong to the "mass class" (roundness index of 0,914), which is characterized by cell organized in a regular manner around the center of the colony (Fig. 4.3). *B16F10* derived spheroids seems to belong instead to the "grape-like class" (roundness index of 0,613, significantly different from the co-culture spheroid with p value = 0.00307) (Fig. 4.3). The grape-like morphology is characterized by colonies with poor cell-cell contacts, responsible of the lack of compactness and grape-like appearance. *B16F10*-spheroid's morphology clearly shows a lack of robust cell-cell adhesion: this evidence has to be overlapped with the absence of collagen type VI, result discussed above (Fig. 4.2A).

To understand how the two cell lines (tumor and fibroblast) distribute in the spheroid, we generate fluorescent spheroids staining *B16F10* with PHK26 (red fluorescence) and *NIH/3T3* with CFSE (green fluorescence) (Fig. 4.4). It seems like the two cell lines distribute homogeneously in the spheroid area, interacting with each other without competition but instead in equilibrium, working in synergy to build an organized structure.
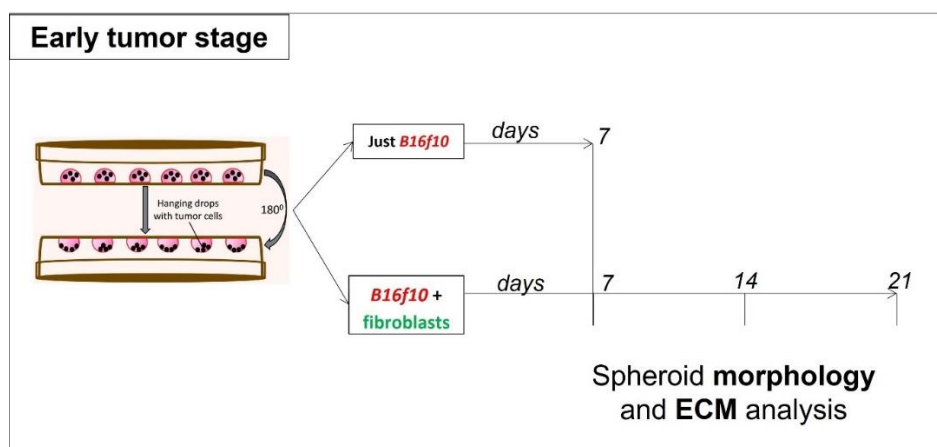

Fig. 4.1. Experimental plan made for analysis of the spheroids. We generate spheroids made by *B16F10* cells and by *B16F10* and *NIH/3T3* cells. At day 7, 14 and 21 analyses of morphology and extracellular matrix deposition were executed. Some spheroids were generated with cells previously stained with a fluorescent dye (PKH26 for *B16F10* and CSFE for *NIH/3T3*) and analyzed with the confocal microscope for cells distribution.
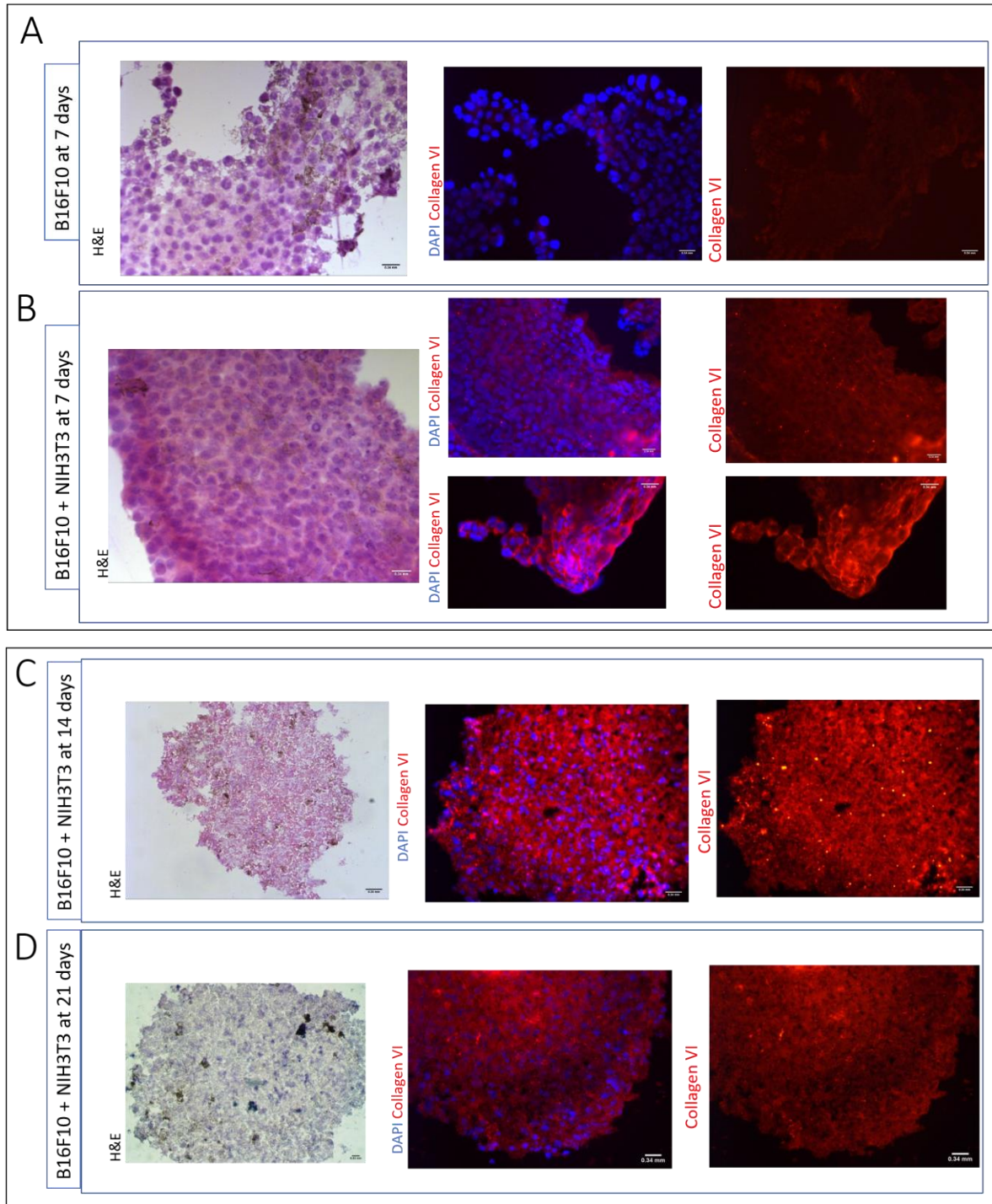
Fig. 4.2. Collagen type VI deposition in spheroids. Left image is representative haematoxylin and eosin staining of spheroid made by *B16F10* cells at day 7 (A), by *B16F10* and *NIH/3T3* cells at day 7 (B), at day 14 (C) and at day 21 (D). Right images are representative of collagen type VI immunostaining (red), with nuclei stained with DAPI (blue). All images were taken with 40x objective. The signal from collagen type VI is barely detectable when the spheroid is made just from *B16F10* cell line. Dapi signal decreases during the time.
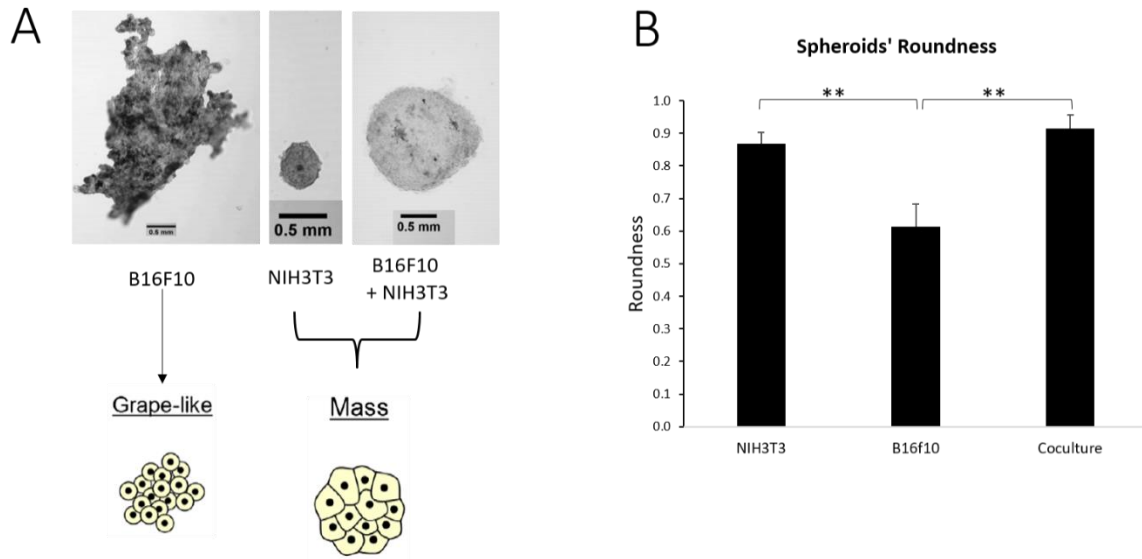
Fig. 4.3. Spheroid morphology classification. (A) Images are representative spheroids made by *B16F10* cells, by *NIH/3T3* cells and by the coculture of both cell line at day 7. The shape let the spheroids be classified in 2 different categories: grape-like for spheroids made by just *B16F10*, and mass like for spheroids made by *NIH/3T3* cells and by the coculture of both cell line. Images were taken taken with 10x objective of a FV500 laser scanning confocal microscope. (B) Measurement of spheroid roundness level from 9 spheroids. As is shown in the graph (Mean ± SD), the roundness level is significantly increased when the fibroblasts are present in the spheroid (p value 0.00307).
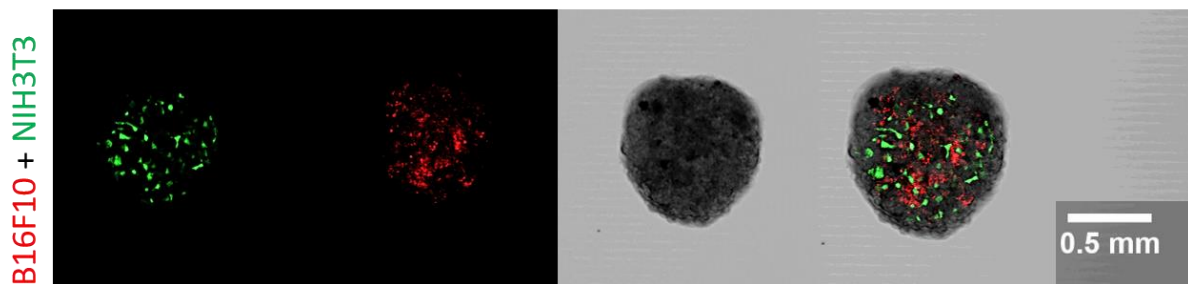

Fig. 4.4. Cells distribution in the spheroid. Images are representative spheroids made by coculture of PKH26-*B16F10* cells and by CFSE-*NIH/3T3* cells, at day 7. The two cell lines distribute homogeneously in the spheroid area. Images were taken taken with 10x objective of a FV500 laser scanning confocal microscope.

Spheroid 3D model shares many biological processes with the in vivo tumor microenvironment

Once we succeeded with the generation of a stable spheroid tumor model, we decided to investigate its gene expression signature. Specifically, we wanted to analyze how much the 3D co-culture model we generated is similar to the *in vivo* microenvironment. We analyzed the gene expression signature of the tumor cell derived from 4 different conditions:
- GFP *B16F10* Linterna[TM] cells 2D cultured;
- GFP *B16F10* Linterna[TM] cells sorted from 2D coculture with fibroblasts;
- GFP *B16F10* Linterna[TM] cells sorted from 3D coculture with fibroblasts;
- *in vivo* tumors generated from GFP *B16F10* Linterna[TM] cells.

Differential expression analysis among all the samples was made using NOIseq[68] and GFold[69]. In Figure 4.5 the heat-map comparing all the genes expressed in the 4 different samples. Not evident similarity or differences among the samples appear clear with this analysis. So we focussed on the genes that were expressed at the same level between the tumor cells derived from the 3D coculture and the actual *in vivo* tumor microenvironment. As the mean-difference plot (MD-plot) shows (Fig. 4.6), 1780 genes were nonregulated (in black dots). The MD-plot is a plot of log-intensity ratios (differences) versus log-intensity averages (means). In this specific MD-plot:
- the red dots having a negative value for the x-axis represent the down regulated genes in the spheroid model compared to the *in vivo* system;
- the red dots having positive value on the x-axis represent the up regulated genes in the spheroid model compared to the *in vivo* system;
- the black dots represent the genes that have the same level of expression in both system (spheroid and *in vivo*).

We selected the genes having the same level of expression between spheroid and *in vivo* model, obtaining a list of 1780 genes. From that list, we excluded the genes having the same expression level analyzing the *in vivo* system signature compere to both the 2D system (*B16F10* cultured alone and with fibroblasts) (Fig. 4.7). The final list, specifying the genes having the same expression level just between spheroid and *in vivo* tumor, is composed by 693 genes.

A KEGG pathway analysis from DAVID was generated from the 693 genes, and a KEGG pathway enrichment dot plot was made (Fig. 4.8 and Table 2). 39 pathways were found being exclusive in both 3D model and tumor *in vivo* and not present during the 2D cultures. 23.1% of the found pathways refers to cancer microenvironment, and the 5.1 % of them refers to the immune system activation, giving grand importance to the spheroid as *in vitro* model compared to the 2D systems. The term "Pathways in cancer" turns out to be the most enriched pathway, highlighting the unique similarity between the spheroid and the *in vivo* environment. 20 genes were reported in this term: EGLN1, RALBP1, FZD3, PTGER1, BRAF, PRKCA, ADCY7, MTOR, CKS1B, NFKBIA, RASSF1, CDK6, CDK4, GNAQ, TRAF5, MAPK1, EP300, ITGA6, VHL, RAF1.
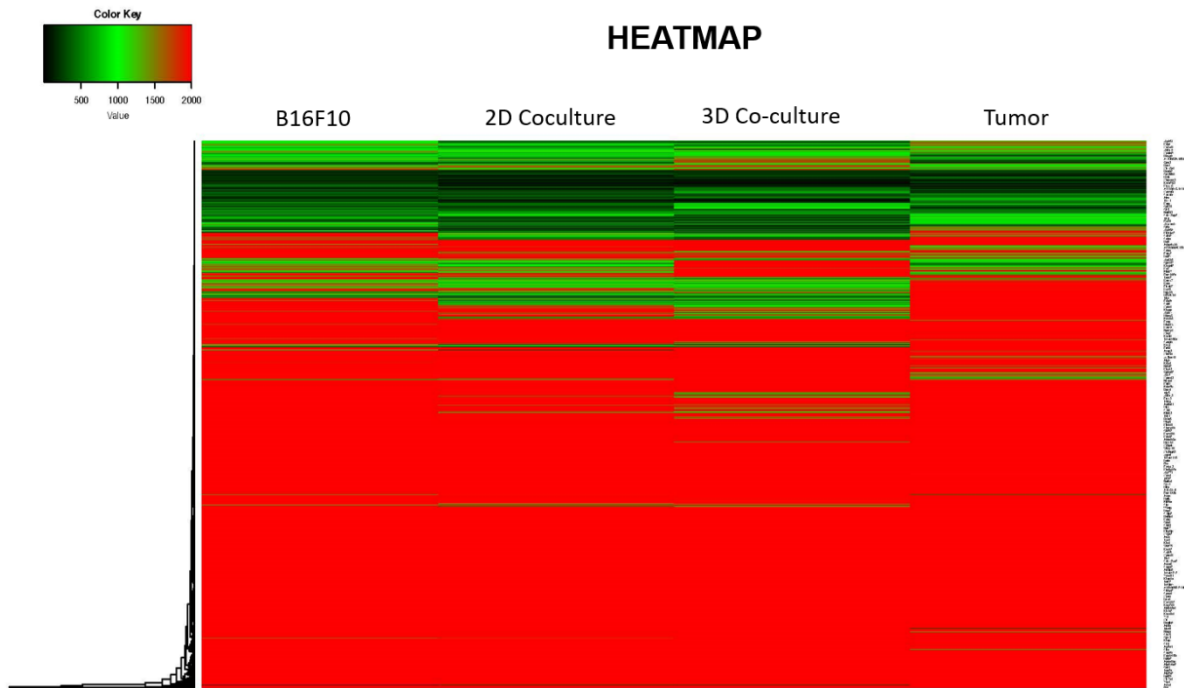
Fig. 4.5. Heat-map of all the genes. The average normalized expression of the B16F10 Control condition between each of the three comparisons was used to generate the heat-map. Not evident similarity or differences among the samples appear clear with this analysis.
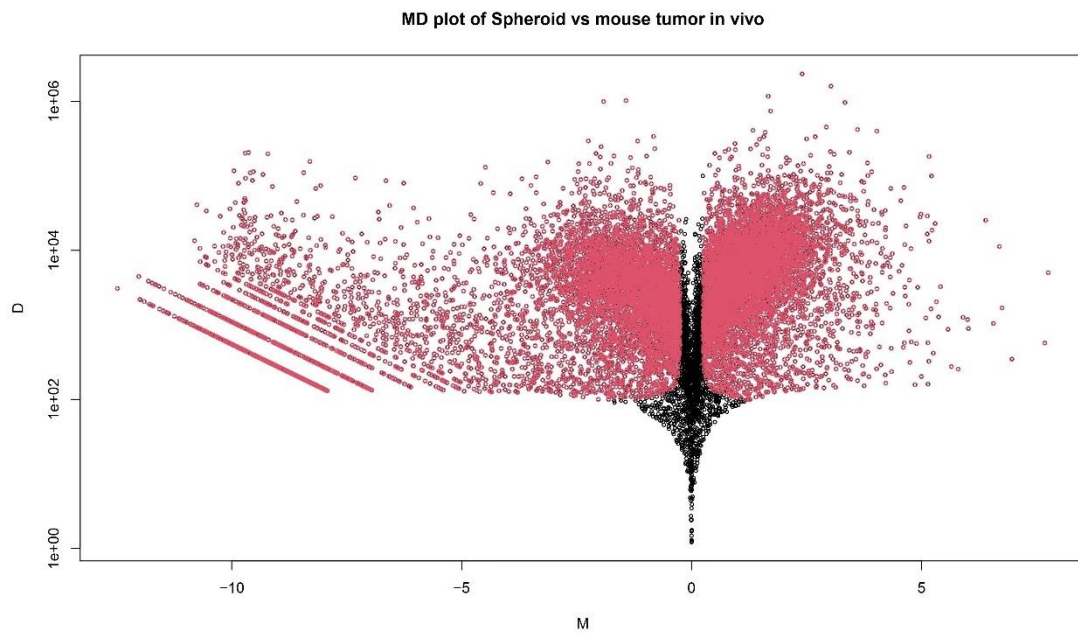

Fig. 4.6. 1780 genes have the same level of expression in spheroid and *in vivo* model. Mean-difference plot (MD-plot) of log-intensity ratios (differences) versus log-intensity averages (means) generated out of the differential expression analysis expression between GFP B16F10 Linterna[TM] cells sorted from 3D coculture with fibroblasts and *in vivo* tumors generated from the same cell line. The plot shows 1780 genes nonregulated (in black dots) which represent the genes with the same level of expression in both the systems.
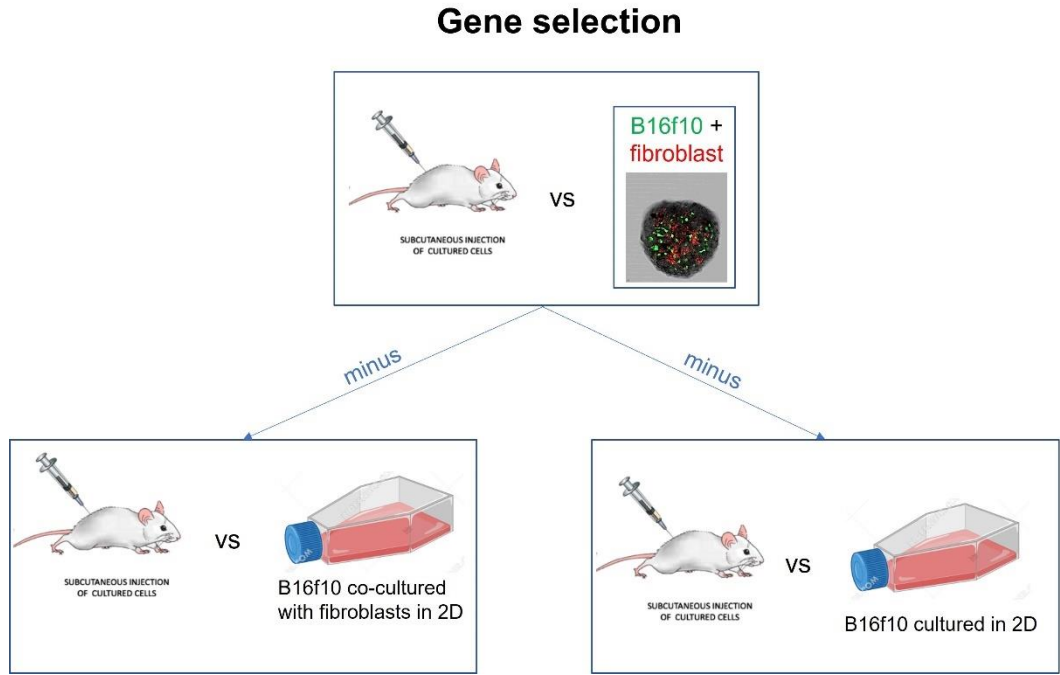
Gene selection

Fig. 4.7. *Modus operandi* **for the gene selection**. For each of the 3 comparison we selected the genes having the same expression level. We obtained 3 lists of genes, one for each comparison. From the list of gene generated from the comparison between GFP B16F10 Linterna™ cells sorted from 3D coculture with fibroblasts and *in vivo* tumors, we removed all the gene present in the other 2 lists of gene generated from the other 2 comparisons. In this way we obtained the specific gene signature in common between spheroid and *in vivo* model.
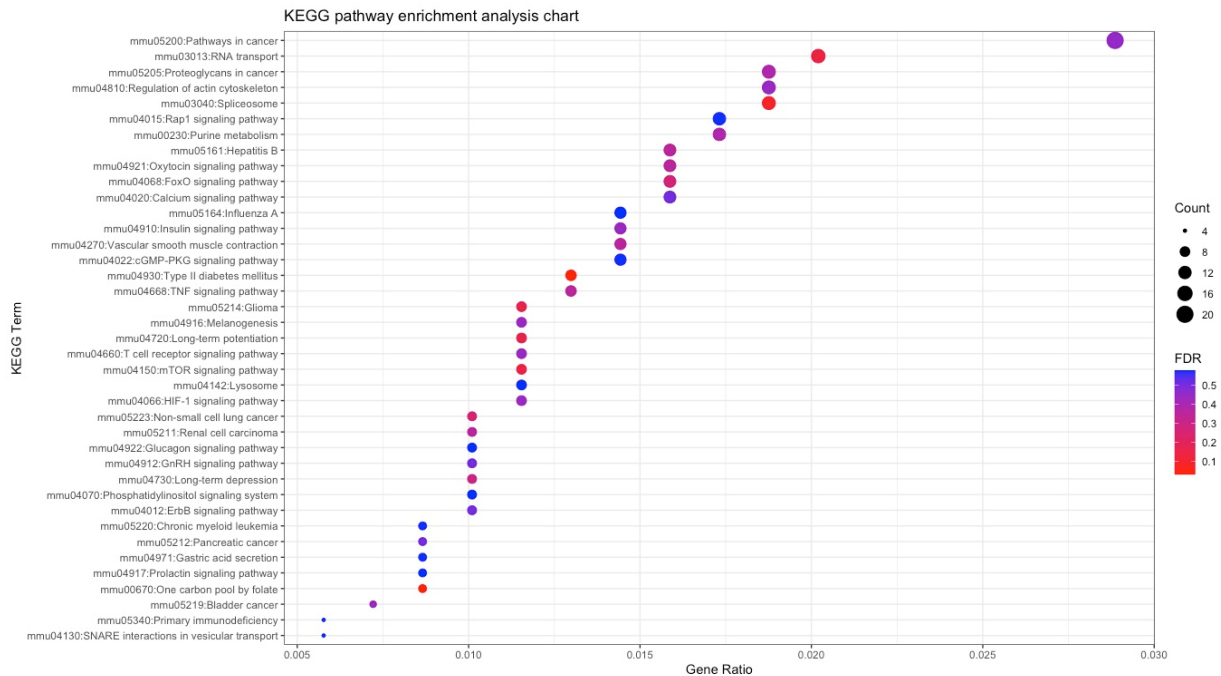

Fig. 4.8. 39 pathways demonstrate the similarity between the 3D model and the tumor *in vivo*. The list of selected 693 genes with same level of expression between B16F10 cells sorted from 3D co-culture with fibroblasts and *in vivo* tumors was analysed with DAVID online platforms for a KEGG pathway analysis. The x-axis (Gene Ratio) is the ratio between the number of genes for each pathway and the total 693 genes. The count legend represents number of genes from the user input genes that are associated in a GO term or pathway. The y-axis (KEGG Term) is the KEGG pathway name. The FDR (False Discovery Rate) legend represent the significance of the data.

Pathway	Count	Pathway	Count
Pathways in cancer	20	Melanogenesis	8
RNA transport	14	T cell receptor signaling pathway	8
Spliceosome	13	HIF-1 signaling pathway	8
Proteoglycans in cancer	13	Lysosome	8
Regulation of actin cytoskeleton	13	Non-small cell lung cancer	7
Purine metabolism	12	Long-term depression	7
Rap1 signaling pathway	12	Renal cell carcinoma	7
FoxO signaling pathway	11	ErbB signaling pathway	7
Hepatitis B	11	GnRH signaling pathway	7
Oxytocin signaling pathway	11	Phosphatidylinositol signaling system	7
Calcium signaling pathway	11	Glucagon signaling pathway	7
Vascular smooth muscle contraction	10	One carbon pool by folate	6
Insulin signaling pathway	10	Pancreatic cancer	6
cGMP-PKG signaling pathway	10	Chronic myeloid leukemia	6
Influenza A	10	Gastric acid secretion	6
Type II diabetes mellitus	9	Prolactin signaling pathway	6
TNF signaling pathway	9	Bladder cancer	5
mTOR signaling pathway	8	SNARE interactions in vesicular transport	4
Glioma	8	Primary immunodeficiency	4
Long-term potentiation	8		

Table 2. 23.1% of the pathways refers to cancer. The list of selected 693 genes with same level of expression between B16F10 cells sorted from 3D coculture with fibroblasts and *in vivo* tumors was analysed with DAVID online platforms for a KEGG pathway analysis. 23.1% of the pathways refers to genes expressed during cancer (in red) and the 5.1% refers to immune system activation (in blue). The "Count" column refers to the found number of genes belonging to the specific pathway.

Decellularization process is efficient on murine melanoma tissue and does not damage the tumor ECM.

To establish a 3D model of an advanced tumor stage, and to the study the decellularizzation process consequences on the tissue structure, murine *B16F10* derived tumors were processed for decellularization, and the generated scaffolds were studied to verify their efficacy as 3D culture system and their extracellular matrix property (Fig. 4.9).

The decellularization process we chosen for this specific tumor spacemen let the tissue keep the extracellular fibers without damage, but at the same time is able to remove all the cells from the tissue, as confirmed by trichrome staining (Fig. 4.10A) and IF analysis of collagen type VI and DNA (Fig. 4.10B).
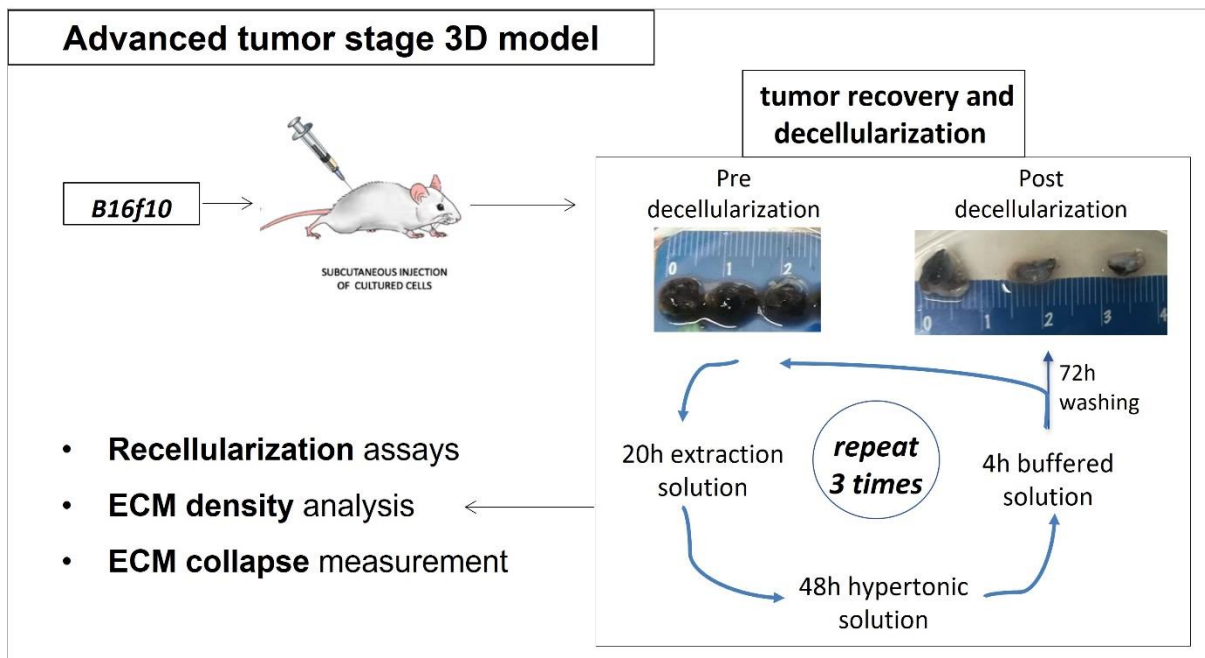

Fig. 4.9. Experimental plan made for analysis of the decellularized tumors. We generate murine tumors made by *B16F10* cells. Tumors were recovered and processed for decellularization. Recellularization assay and ECM analysis were performed.
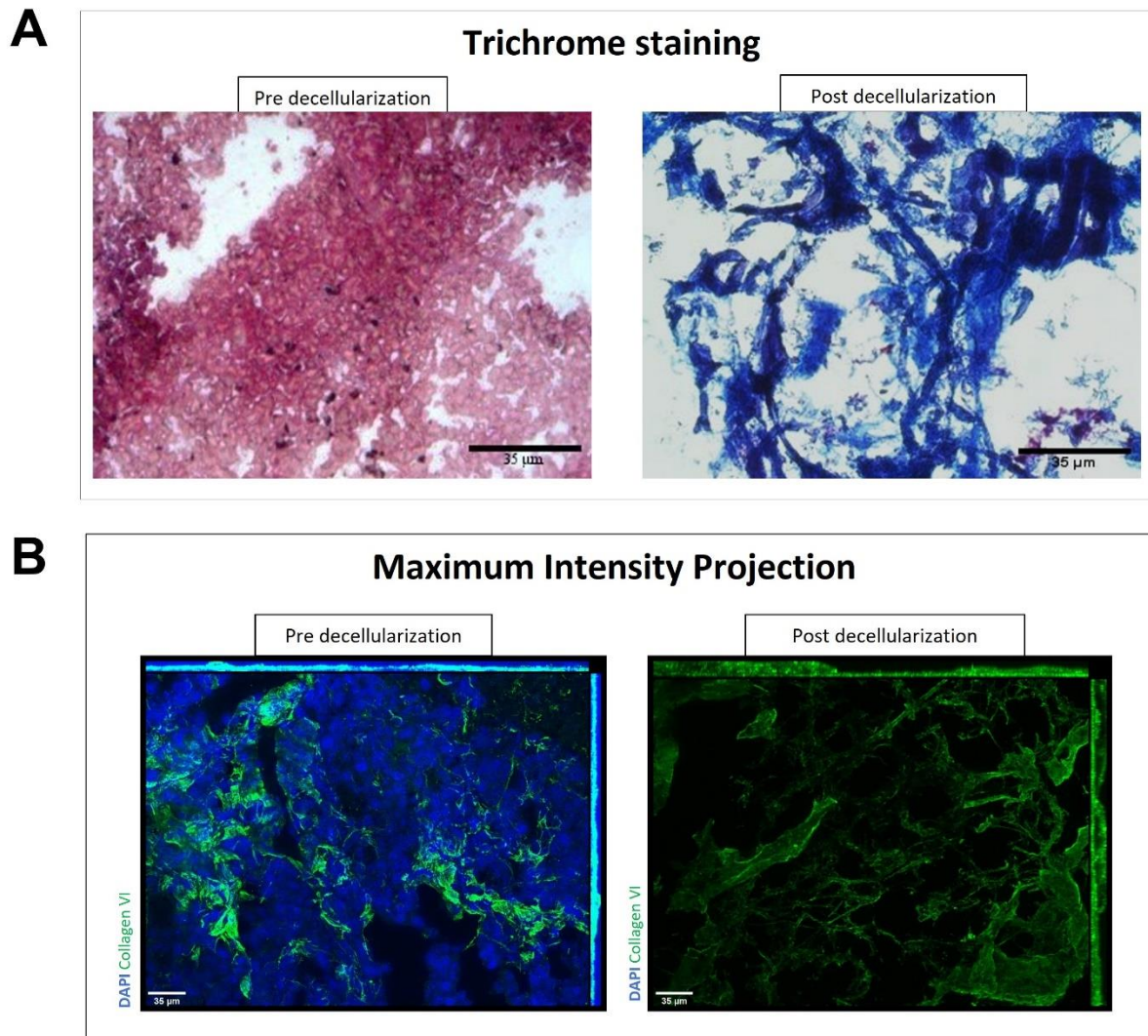
Fig. 4.10. **Decellularization process is successful**. (A) Representative Mallory trichrome staining of murine melanoma tumor tissue decellularized (right) and fresh not decellularized (left). The decellularization process is able to remove all of cells from the tissue and does not take away the ECM. Scale bar 35 µm. (B) Representative maximum intensity projections (MIP) of deconvoluted images acquired with an Axio Imager A2M microscope equipped with an apotome module of collagen type VI immunostaining (green) of murine melanoma tumor tissue decellularized (right) and fresh not decellularized (left). Nuclei were stained with DAPI (blue) Scale bar 35 µm.

Recellularization is limited to tissue border.

To test the efficacy of the decellularized tissue as scaffolds for 3D culture, we executed a 7 days recellularization experiment with *B16F10* or *NIH/3T3* cell lines. As expected, cell attachment was limited to the border of the tissue (Fig. 4.11). We also tested if the co-culture of the two cell lines could have permitted a better recellularization of the obtained matrix. Cell recellularization was limited to tissue border also in this case. The partial recellularization has been also observed cultivating *ex vivo* murine melanoma derived cells on the decellularized tissue. Control experiment with polyurethane demonstrate the capability of *B16F10* and *NIH/3T3* cell lines to infiltrate a synthetic matrix, with porosity between 200 and 630 µm (Fig. 4.12).
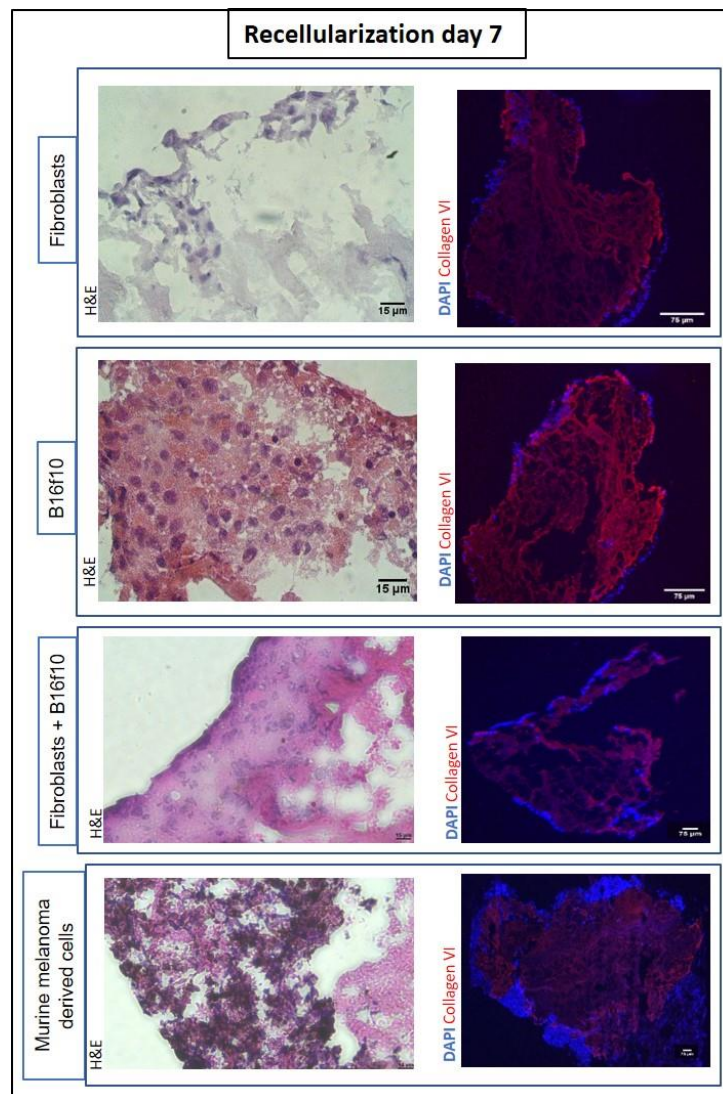

Fig. 4.11. **Recellularization is limited to tissue border.** Left images are representative haematoxylin and eosin staining of murine tumor derived scaffold recellularized with *B16F10* cells (first box), *NIH/3T3* cells (second box), the co-culture of the two cell lines (third box) and murine melanoma derived cells (fourth box) at 7 days of culture (scale bar 15 µm). Right images are representative of collagen type VI immunostaining (red) of same samples, with nuclei stained with DAPI (blue) and scale bar 75 µm. Cells appear to be localized mostly at the border of the scaffold.
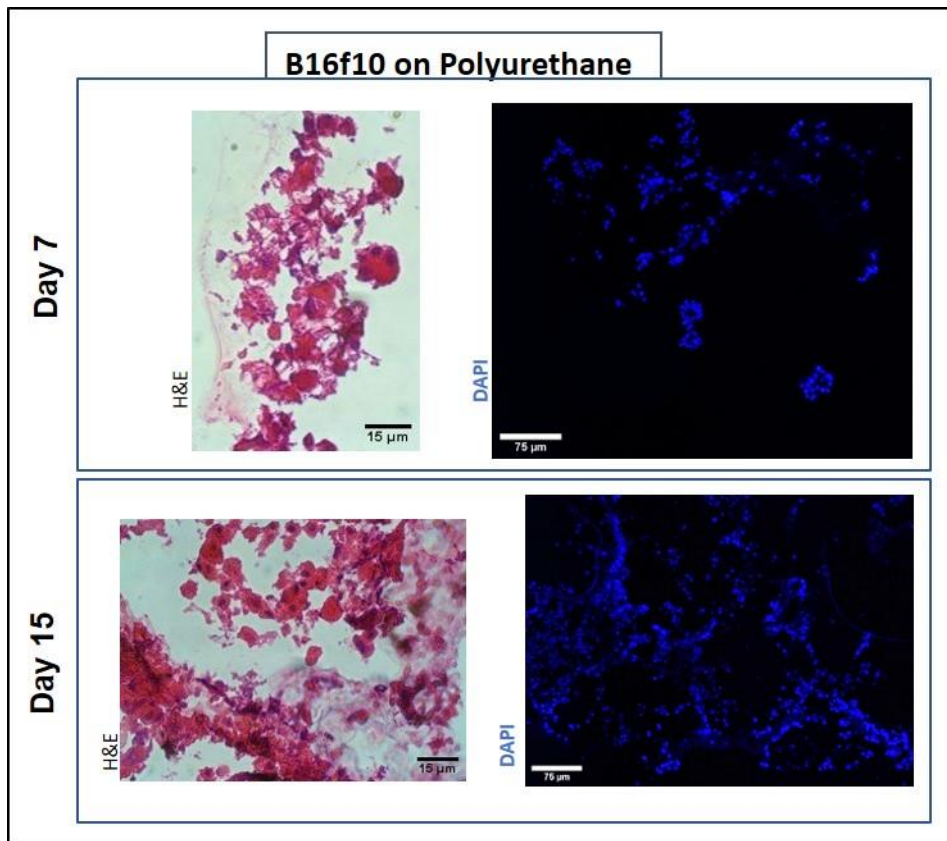
Fig. 4.12. B16f10 and NIH/3T3 cell lines infiltrate Polyurethane synthetic matrix Left images are representative haematoxylin and eosin staining of Polyurethane scaffold recellularized with *B16F10* cells at day 7 (top of the figure) and day 15 (bottom of the figure), with scale bar of 15 µm. Right images are representative images of same samples, with nuclei stained with DAPI (blue) and scale bar 75 µm. Cells appear to be localized overall the scaffold.

Decellularization process provokes collapse of the ECM.

20 µm frozen sections of decellularized and fresh tumor tissue were analyzed for detection of collagen type VI by Z-stacking method, which can virtually decompose the whole section in more surfaces and analyze the immunofluorescence signal separately for each surface. The Z-stack analysis (Fig. 4.13) showed an increase of ECM in the decellularized tissue compared to the not decellularized one. The mass reduction of the tissue after decellularization is clear also at the macroscopic view of the tissues (Fig. 4.14).

The observation through the scanning electron microscope (SEM) explains the morphology of the induced murine tumor by *B16F10* cell line (Fig. 4.15A): the tissue appears with a multitude of cells which makes difficult the observation of the fibres. Only after the decellularization treatment the extracellular fibres are exposed: the lack of cells makes the fibres twist on themselves, generating a complex net. This phenomenon is better visible on a human decellularized melanoma (Fig. 4.15B) which is a tissue with a higher quantity of fibres compared to an induced murine tumor. The collapse of the extracellular matrix following the decellularizing treatment is better detectable on a tissue having a geometric structure, like the pulmonary parenchyma: here the collapse of the ECM is measurable through alveoli area reduction (p value 0.013) (Fig. 4.16).
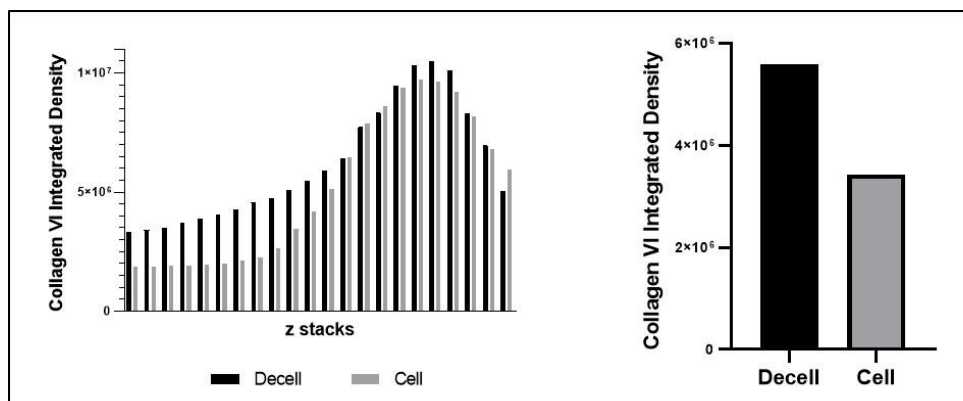

Fig. 4.13. Increasing of ECM in the decellularized sample. Measurement of collagen type VI immunostaining integrated density of each z stacks (left graph) from 20 µm section of murine melanoma samples decellularized (black columns) and fresh not decellularized (gray columns). In the graph on the right: measurement of collagen type VI immunostaining integrated density of the maximum intensity projection of 20 µm section of murine melanoma samples decellularized (black column) and fresh not decellularized (gray column). The decellularized sample shows a clear increasing of ECM.
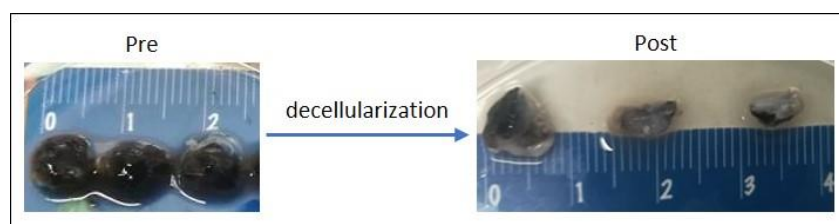

Fig. 4.14. Reduction of the tissue after decellularization Representative images of approximately 3x3x1 mm murine melanoma piece, before and after the process. The decreasing of mass and the loss of color is clear comparing the samples before and after the decellularization treatment.
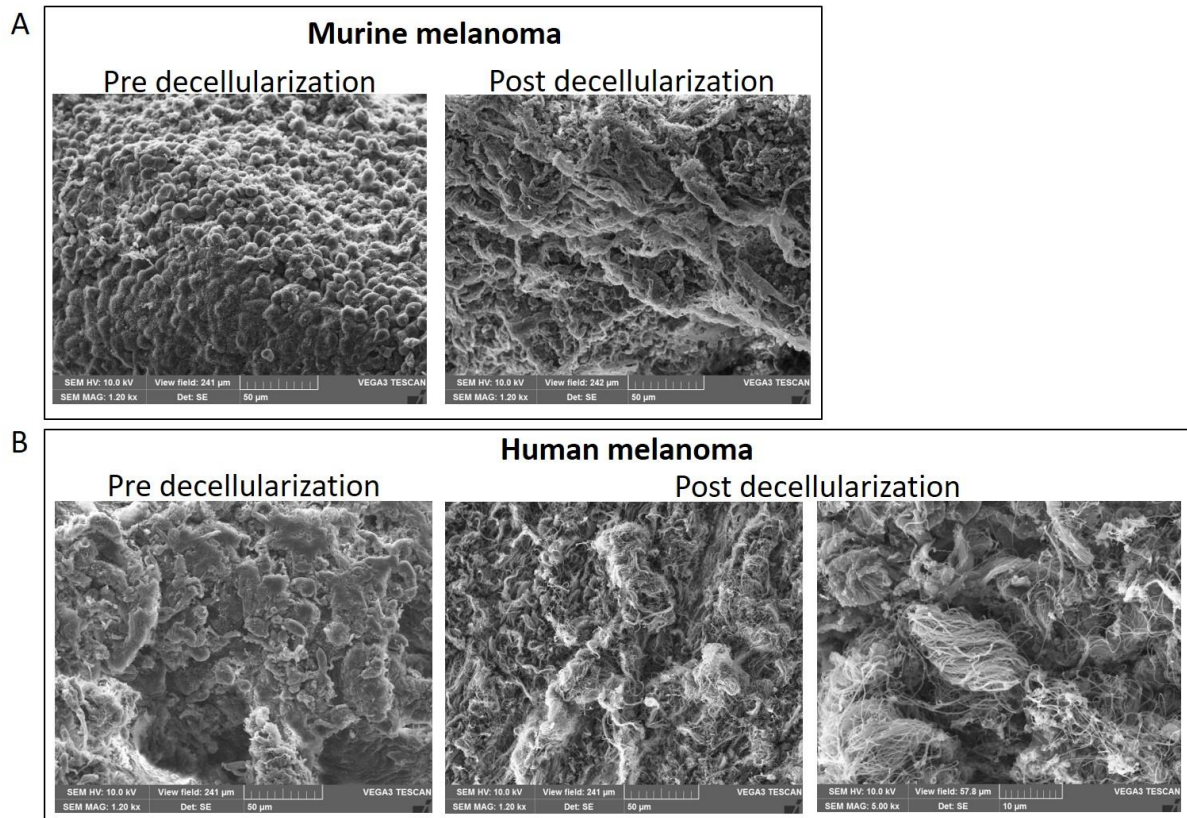
Fig. 4.15. Decellularization process generates a complex net of fibers. Representative scanning electron images of murine melanoma samples (A) and human melanoma sample (B) before and after the decellularization process. After the decellularization treatment the extracellular fibres are exposed: the lack of cells makes the fibres twist on themselves, generating a complex net, impenetrable from cells. The decellularized melanoma shows a thick net of fibres which seem twist on themselves due to the loss of cells that fibres are meant to support.
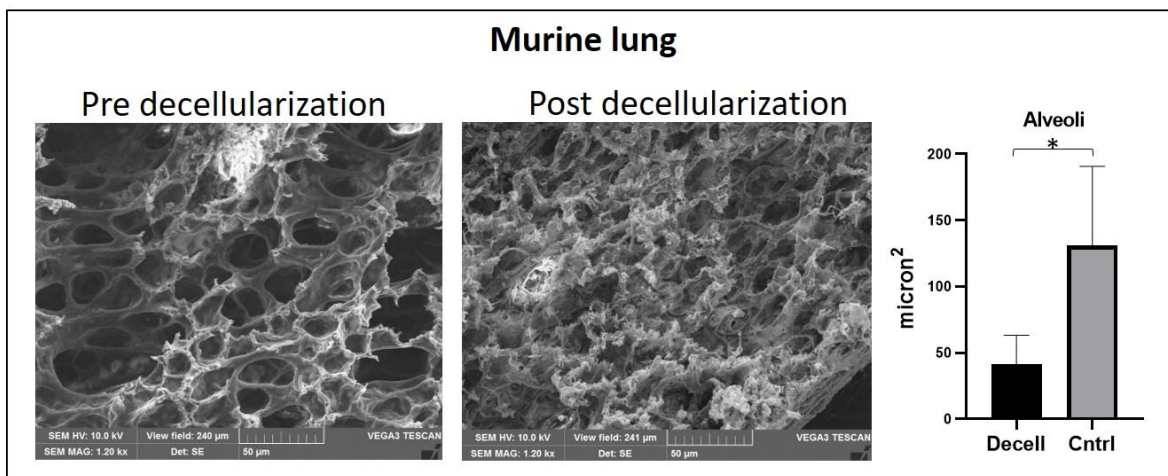

Fig. 4.16. ECM collapse measurement. Representative scanning electron images of mouse lung samples before and after the decellularization process. As is shown in the graph (Mean ± SD), the collapse of the ECM is measurable through alveoli area reduction (p value 0.013).

5. Discussion

The study of the microenvironment is becoming an essential need in oncology field. However, the *in vitro* techniques providing a model that incorporates the extracellular matrix are still in a developing era. In this work, we show the importance of the ECM for *in vitro* experimentations and the difficulties that still need to be overstep.

First, we decided to develop a model able to mimic a tumor environment during its first stage. Spheroids are a popular model that can very well satisfy this request. Moreover, with this model, we were also able to provide ECM to the *in vitro* system. Indeed, we developed and analysed different kind of spheroids made by just tumor cells or co-culture of tumor and fibroblast cells. We noticed that spheroids generated by the co-culture of *B16F10* and *NIH/3T3* cells were the only ones where the extracellular matrix was detected and the only ones lasting for more than one week, up to 21 days (Fig. 4.2). These results let deduce that ECM deposition is feasible in the spheroid model and that it is fibroblast dependent.

Taking a better look to the spheroids' morphology, we discover that *B16F10 + NIH/3T3* derived spheroids belong to the "mass" class (Fig. 4.3), which is characterized by cells organized in a regular manner around the center of the colony. *B16F10* derived spheroids seems to belong instead to the "grape-like" class, characterized by colonies with poor cell-cell contacts and distinguished by their grape-like appearance. *B16F10*-spheroid's morphology clearly shows a lack of robust cell-cell adhesion, result that must be overlapped with the absence of collagen type VI (Fig. 4.3). These results let us deduce again that ECM deposition is fibroblast dependent. Therefore, fibroblasts are needed for the generation of an early tumor stage 3D model because of their major role as ECM producers and tumor micro-environment organizers [70]. Moreover, to understand how the two cell lines (tumor and fibroblast) distribute in the spheroid, we generate fluorescent spheroids staining *B16F10* with PHK26 (red fluorescence) and *NIH/3T3* with CFSE (green fluorescence). Looking at the Fig. 4.4, we deduced that he two cell lines distribute homogeneously in the spheroid area, interacting with each other without any competition but instead in equilibrium, working in synergy to build an organized structure.

Once we succeeded with the generation of a stable spheroid tumor model, we decided to investigate its gene expression signature. We focussed on the genes that were expressed at the same level between the tumor cells derived from the 3D co-culture and the actual *in vivo* tumor microenvironment in order to find how much our 3D model is similar to an *in vivo* scenario, based the gene expression. Clusters analysis highlights the similarity between the 2 groups showing specific pathways (Table 2 and Fig. 4.8). The term "Pathways in cancer" turns out to be the most enriched pathway, highlighting the unique similarity between the spheroid and the *in vivo* environment. 20 genes were reported in this term: EGLN1, RALBP1, FZD3, PTGER1, BRAF, PRKCA, ADCY7, MTOR, CKS1B, NFKBIA, RASSF1, CDK6, CDK4, GNAQ, TRAF5, MAPK1, EP300, ITGA6, VHL, RAF1. This result highlights the importance of utilizing 3D model for tumor experimentation: when the tumor cell is co-cultivated with a fibroblast line and following 3D condition, it shows similarity with the actual tumor microenvironment on the expression of genes belonging especially to the tumor scenario. The lack of the real tumor signature of cancer cells cultured in 2D is actually one of the major limits of culture method. High level of gene enrichment is gained also from the pathways involving the regulation of the immune system (*mTOR signaling pathway and T cell receptor signaling pathway*), meaning that the 3D model has more chance to be immunologically regulated in the same way as the *in vivo* tumor is. In summary, preferring 3D culture methods might definitely

be the key for a better drug screening. Indeed, 2D cultured tumor cells appear to be sensitive for certain kind of drugs, but often those selected treatments fall to be effective in a real environment like the cancer harboring patient.

Due to the day-by-day loss of vitality observed in the spheroid model (loss of DAPI signal in Fig. 4.2), for the development of a 3D tumor model lasting for more weeks, another culture model is required. Tumor derived 3D scaffolds seem to be the tool which most truthfully represents the real *in vivo* scenario of a tumor microenvironment. Anyway, the generation of decellularized tumor scaffolds is still an ongoing challenge, especially for the low rate of recellularizzation. Indeed, in many studies the fresh decellularized matrices are lyophilized and processed to become hydrogel scaffolds, which provide the porosity needed for a proper recellularizzation [52,58,63]. Actually, the reasons of a lacking recellularizzation are still not well investigated. Here in this work, we reported our experience on the generation of a scaffold made by murine tumor tissue and we analyze the ECM before and after the decellularization treatment. During all the experiments, we have chosen to analyze the ECM by the detection of collagen type VI since is a widely distributed extracellular matrix protein highly expressed in a variety of cancers, as well as in the *B16F10* derived tumor, the model we are studying [71,72].

Once we obtained the tumor derived scaffold, we tested their capability of being colonized by cells executing different recellularization experiments. In first place, we have chosen to culturing on the obtained scaffold the two different cell lines we used for spheroid generation, *B16F10* tumor cell line, and *NIH/3T3* fibroblast cell line. With this choice we exanimated the scaffold attachment capability of two cell line with different features, since one is a tumor (*B16F10*) cell line and the other one belongs to the matrisome (*NIH/3T3*). However, after 7 days of culture, for both cell lines the attachment was limited just to the border of the tissue (Fig. 4.11), as already described in literature [52–54]. We also tested if the co-culture of the two cell lines could have permitted a deeper recellularization of the scaffold. It has known that *B16F10* melanoma cells are able to stimulate *NIH3T3* fibroblasts to exhibit the characteristics of cancer stem-like cells (CSCs) [70]. Therefore, the co-culture of these two cell lines at the same time on the decellularized tumor might have generate a synergic effect enabling tissue cell penetration, also due to the combination of the high proliferation rate of tumor cells and the attachment capability of fibroblasts. Even in this case, cell recellularization was limited to tissue border in this case as well. As last recellularization test, we cultivated *ex vivo* cells recovered from murine melanoma tumor. *Ex vivo* cells are supposed to be more aggressive and able to produce metalloproteases helpful for matrix penetration, but the partial recellularization was observed in this case as well, meaning that neither *ex vivo* tumor environment cells are able to colonize the decellularized tissue. Control experiment with polyurethane, often used scaffold due to the recellularization suitability [73], demonstrated the capability of *B16F10* and *NIH/3T3* cell lines to infiltrate the synthetic matrix (Fig. 4.12).

With these evidences we deduced that, as expected, cells are not able to pass through the ECM of the tumor scaffold that we generated by decellularization, confirming the limit of the technique. The lack of inner recellularization of the generated scaffold might be due to the collapse of the ECM that may follow the decellularization process. To have a better understanding of the ECM structure, we moved forward with morphology analysis of fresh and decellularized samples. As expected, the Z-stack analysis (Fig. 4.13) showed an increase of ECM in the decellularized tissue compared to the not decellularized one. This result encourages

our hypothesis of a collapse of the tumor ECM structure after the treatment, since cells are removed from the environment and the matrix does not need to support them anymore. Indeed, the mass reduction of the tissue after the decellularization treatment is clear also at the macroscopic view of the pieces (Fig. 4.14). We implemented the ECM observation with the support of the Scanning Electron Microscopy (SEM). SEM allowed us to better understand the overall morphology of the induced murine tumor by *B16F10* cell line (Fig. 4.15A): the tissue appears with a multitude of cells which make arduous the observation of the fibres. But after the decellularization treatment the extracellular fibres are exposed and it is possible to take a closer look to the structure: as hypothesized, the lack of cells makes the fibres twist on themselves, generating a complex net, probably impenetrable from cells (Fig. 4.15A). The same phenomenon was visible even better on a human decellularized melanoma spaceman (Fig. 4.15B). This amplification of the phenomenon could be explained since the human tumor is a tissue with a higher quantity of fibres compared to an induced murine tumor, probably due to the different time occurring for the tumor development (the tumor generated in the mouse is already detectable just few days after the tumor cell injection). The decellularized human melanoma SEM view shows a thick net of fibres seeming twist on themselves, given the loss of cells which fibres are meant to support. Looking at the pictures (Fig. 4.15), it is really easy understand the impossibility of cell penetration after decellularization treatment.

In order to create a method to measure the collapse of the extracellular matrix that a decellularization treatment may provokes, we compared a fresh and a decellularized specimen of mouse pulmonary parenchyma, since it is a tissue with a geometric and organized structure, where structural modifications are easy to be detected. In this way we were able to quantify the collapse of the ECM through alveoli area reduction (Fig.4.16). As much as we know, nobody until now has ever provided a method to measure the collapse that the dececellurarization process might provoke on the spacemen. The method we are proposing here is a new and useful test to easy predict and quantify the modification that the process might provoke on precious samples.

6. Conclusion

The development of the spheroid made by tumor and fibroblast cells is a more realistic environment compared to the usual 2D culture and to the spheroid made simply by tumor cells. Fibroblasts are needed for the generation of a better 3D model because of their major role as ECM producers and tumor micro-environment organizers. The combination of the two different cell lines helps to understand how the interaction between them can impact the tumor growth. The spheroid model is suitable for many studies, like the study of cell 3D morphology, ECM deposit, cell signalling. The limit of the spheroid model is the time, since, to date, the system does not provide oxygen import, necessary for the tumor bulk growth. Tumor derived 3D scaffolds by decellularization most truthfully represents the real *in vivo* scenario of a tumor 3D model, but the recellularization lack is very often a big limit. Our data demonstrate that the decellularizzation process provokes the collapse of the matrix that does not allow the tissue to be utilized as scaffold for *in vitro* cell experimentation. Here we also provide, for the first time, a method to test the damage that the treatment provokes on the samples, avoiding the loss of precious materials.

Since this field of research has still few knowledge and the protocols are not yet standardized, this work will be one of the milestones for the future of the 3D *in vitro* cell culture. More research must be done to find the optimal conditions for tumor samples to become usable scaffolds, since this source is the only one providing the real *in vivo* representation of the tumor microenvironment. A considerable idea for decellularized tissue cell colonization can be utilizing a bioreactor, a millifluidic system, consisting of a transparent culture chamber featured with a flow inlet and outlet for the profusion of the cell culture media. Our idea is to challenge the scaffold with a culture media featured by tumor cells, matrisoma cells and even splenocytes, to understand if the model is able to recruit immune system cells. The success of this system will even represent an alternative option to *in vivo* experimentation, or at least its reduction.

The decellularization process helps to support the idea of a human 3D culture system personalized for each patient affected by neoplasia. The ideal 3D model, indeed, would be made by tissues derived from the patient tumor biopsy, which will allow to test *in vitro* different chemo/immunotherapeutic treatments on the specific patient tissue before the administration of the drugs to the actual patient. Only with ECM features the 3D model will allow to better predict the outcome of different treatments, and will eventually drive the physician to an efficient and personalized drug therapy.

7. Bibliography

1. Eskiizmir G, Özgür E. Epithelial-Mesenchymal Transition in Tumor Microenvironment Induced by Hypoxia. *Cancer Metastasis*. Published online November 5, 2018. doi:10.5772/INTECHOPEN.78717
2. JM L, S D, R K, EW T. The epithelial-mesenchymal transition: new insights in signaling, development, and disease. *J Cell Biol*. 2006;172(7):973-981. doi:10.1083/JCB.200601018
3. R K, EG N. Epithelial-mesenchymal transition and its implications for fibrosis. *J Clin Invest*. 2003;112(12):1776-1784. doi:10.1172/JCI20530
4. A D, C G, G G. The stroma reaction myofibroblast: a key player in the control of tumor cell behavior. *Int J Dev Biol*. 2004;48(5-6):509-517. doi:10.1387/IJDB.041802AD
5. Sahai E, Astsaturov I, Cukierman E, et al. A framework for advancing our understanding of cancer-associated fibroblasts. *Nat Rev Cancer*. 2020;20(3):174. doi:10.1038/S41568-019-0238-1
6. F X, J S, K W. Cancer associated fibroblasts (CAFs) in tumor microenvironment. *Front Biosci (Landmark Ed*. 2010;15(1):166-179. doi:10.2741/3613
7. SE W, H S, F L, et al. Enhancement of head and neck squamous cell carcinoma proliferation, invasion, and metastasis by tumor-associated fibroblasts in preclinical models. *Head Neck*. 2014;36(3):385-392. doi:10.1002/HED.23312
8. JP T. Epithelial-mesenchymal transitions in tumour progression. *Nat Rev Cancer*. 2002;2(6):442-454. doi:10.1038/NRC822
9. J Y, RA W. Epithelial-mesenchymal transition: at the crossroads of development and tumor metastasis. *Dev Cell*. 2008;14(6):818-829. doi:10.1016/J.DEVCEL.2008.05.009
10. H A, MS A, K F, M B-F, MA N. Epithelial-mesenchymal transitions: the importance of changing cell state in development and disease. *J Clin Invest*. 2009;119(6):1438-1449. doi:10.1172/JCI38019
11. J Y, D W, P W, Z C, J H. The cancer stem cell niche: cross talk between cancer stem cells and their microenvironment. *Tumour Biol*. 2014;35(5):3945-3951. doi:10.1007/S13277-013-1561-X
12. Ayob AZ, Ramasamy TS. Cancer stem cells as key drivers of tumour progression. *J Biomed Sci 2018 251*. 2018;25(1):1-18. doi:10.1186/S12929-018-0426-4
13. Sell S. On the Stem Cell Origin of Cancer. *Am J Pathol*. 2010;176(6):2584. doi:10.2353/AJPATH.2010.091064
14. SH M, EG L. Multistage carcinogenesis and the incidence of human cancer. *Genes Chromosomes Cancer*. 2003;38(4):302-306. doi:10.1002/GCC.10264
15. BB T, R B. Cancer initiation and progression: involvement of stem cells and the microenvironment. *Biochim Biophys Acta*. 2007;1775(2):283-297. doi:10.1016/J.BBCAN.2007.01.001
16. Demaria S, Pikarsky E, Karin M, et al. Cancer and Inflammation: Promise for Biological Therapy. *J Immunother*. 2010;33(4):335. doi:10.1097/CJI.0B013E3181D32E74
17. H L, W O, C H. Inflammation, a key event in cancer development. *Mol Cancer Res*. 2006;4(4):221-233. doi:10.1158/1541-7786.MCR-05-0261
18. F O. Inflammation and free radicals in tumor development and progression. *Redox Rep*. 2002;7(6):357-368. doi:10.1179/135100002125001135
19. Ohnishi S, Ma N, Thanan R, et al. DNA damage in inflammation-related carcinogenesis and cancer stem cells. *Oxid Med Cell Longev*. Published online 2013. doi:10.1155/2013/387014
20. Muz B, De La Puente P, Azab F, Azab AK. Hypoxia Dovepress The role of hypoxia in cancer progression, angiogenesis, metastasis, and resistance to therapy. Published online 2015. doi:10.2147/HP.S93413
21. Tian L, Goldstein A, Wang H, et al. Mutual regulation of tumour vessel normalization and immunostimulatory reprogramming. *Nature*. 2017;544(7649):250-254. doi:10.1038/nature21724
22. EY L, NP H, TK L. Cancer Stem Cells and Their Microenvironment: Biology and Therapeutic Implications. *Stem Cells Int*. 2017;2017. doi:10.1155/2017/3714190

23. Stoddart RW. The Generation of Cancer: Initiation, promotion, progression and the multiple influences of the environment: *http://dx.doi.org/101177/026010608300200405*. 2016;2(3-4):153-162. doi:10.1177/026010608300200405

24. Deshmukh S, Saini S. Phenotypic Heterogeneity in Tumor Progression, and Its Possible Role in the Onset of Cancer. *Front Genet*. 2020;0:1525. doi:10.3389/FGENE.2020.604528

25. Fischer EG. Nuclear Morphology and the Biology of Cancer Cells. *Acta Cytol*. 2020;64(6):511-519. doi:10.1159/000508780

26. Baba AI, Câtoi C. TUMOR CELL MORPHOLOGY. Published online 2007. Accessed July 23, 2021. https://www.ncbi.nlm.nih.gov/books/NBK9553/

27. Frank SA, Rosner MR. Nonheritable Cellular Variability Accelerates the Evolutionary Processes of Cancer. *PLOS Biol*. 2012;10(4):e1001296. doi:10.1371/JOURNAL.PBIO.1001296

28. Pustylnikov S, Costabile F, Beghi S, Facciabene A. Targeting mitochondria in cancer: current concepts and immunotherapy approaches. *Transl Res*. 2018;202. doi:10.1016/j.trsl.2018.07.013

29. Leung KK, Wilson GM, Kirkemo LL, Riley NM, Coon JJ, Wells JA. Broad and thematic remodeling of the surfaceome and glycoproteome on isogenic cells transformed with driving proliferative oncogenes. *Proc Natl Acad Sci U S A*. 2020;117(14):7764-7775. doi:10.1073/PNAS.1917947117/-/DCSUPPLEMENTAL

30. Salvador E, Burek M, Förster CY. Tight Junctions and the Tumor Microenvironment. *Curr Pathobiol Reports 2016 43*. 2016;4(3):135-145. doi:10.1007/S40139-016-0106-6

31. Winkler J, Abisoye-Ogunniyan A, Metcalf KJ, Werb Z. Concepts of extracellular matrix remodelling in tumour progression and metastasis. *Nat Commun 2020 111*. 2020;11(1):1-19. doi:10.1038/s41467-020-18794-x

32. Wells JM, Gaggar A, Blalock JE. MMP generated matrikines. *Matrix Biol*. 2015;44-46:122-129. doi:10.1016/J.MATBIO.2015.01.016

33. Jenkins RW, Aref AR, Lizotte PH, et al. Ex vivo profiling of PD-1 blockade using organotypic tumor spheroids. *Cancer Discov*. 2018;8(2):196-215. doi:10.1158/2159-8290.CD-17-0833

34. Bourland J, Fradette J, Auger FA. Tissue-engineered 3D melanoma model with blood and lymphatic capillaries for drug development. *Sci Rep*. 2018;8(1). doi:10.1038/s41598-018-31502-6

35. Amann A, Zwierzina M, Koeck S, et al. Development of a 3D angiogenesis model to study tumour - endothelial cell interactions and the effects of anti-angiogenic drugs. *Sci Rep*. 2017;7(1). doi:10.1038/s41598-017-03010-6

36. Ganesan MK, Finsterwalder R, Leb H, et al. Three-dimensional coculture model to analyze the cross talk between endothelial and smooth muscle cells. *Tissue Eng - Part C Methods*. 2017;23(1):38-49. doi:10.1089/ten.tec.2016.0299

37. Cox TR, Erler JT. Remodeling and homeostasis of the extracellular matrix: Implications for fibrotic diseases and cancer. *DMM Dis Model Mech*. 2011;4(2):165-178. doi:10.1242/dmm.004077

38. Horning JL, Sahoo SK, Vijayaraghavalu S, et al. 3-D tumor model for in vitro evaluation of anticancer drugs. *Mol Pharm*. 2008;5(5):849-862. doi:10.1021/mp800047v

39. Dondajewska E, Juzwa W, Mackiewicz A, Dams-Kozlowska H. Heterotypic breast cancer model based on a silk fibroin scaffold to study the tumor microenvironment. *Oncotarget*. 2018;9(4):4935-4950. doi:10.18632/oncotarget.23574

40. Melissaridou S, Wiechec E, Magan M, et al. The effect of 2D and 3D cell cultures on treatment response, EMT profile and stem cell features in head and neck cancer. *Cancer Cell Int*. 2019;19(1):16. doi:10.1186/s12935-019-0733-1

41. Fontoura JC, Viezzer C, dos Santos FG, et al. Comparison of 2D and 3D cell culture models for cell growth, gene expression and drug resistance. *Mater Sci Eng C*. 2020;107. doi:10.1016/j.msec.2019.110264

42. Ghosh S, Spagnoli GC, Martin I, et al. Three-dimensional culture of melanoma cells profoundly affects gene expression profile: A high density oligonucleotide array study. *J Cell Physiol*. 2005;204(2):522-531. doi:10.1002/jcp.20320

43. Białkowska K, Komorowski P, Bryszewska M, Miłowska K. Spheroids as a Type of Three-

Dimensional Cell Cultures—Examples of Methods of Preparation and the Most Important Application. *Int J Mol Sci*. 2020;21(17):1-17. doi:10.3390/IJMS21176225

44. E C, A M, C M. Scaffolds for tissue engineering and 3D cell culture. *Methods Mol Biol*. 2011;695:17-39. doi:10.1007/978-1-60761-984-0_2

45. Nyga A, Loizidou M, Emberton M, Cheema U. A novel tissue engineered three-dimensional in vitro colorectal cancer model. *Acta Biomater*. 2013;9(8):7917-7926. doi:10.1016/j.actbio.2013.04.028

46. Lu P, Weaver VM, Werb Z. The extracellular matrix: A dynamic niche in cancer progression. *J Cell Biol*. 2012;196(4):395-406. doi:10.1083/jcb.201102147

47. Malik R, Lelkes PI, Cukierman E. Biomechanical and biochemical remodeling of stromal extracellular matrix in cancer. *Trends Biotechnol*. 2015;33(4):230-236. doi:10.1016/j.tibtech.2015.01.004

48. Naba A, Clauser KR, Hoersch S, Liu H, Carr SA, Hynes RO. The matrisome: In silico definition and in vivo characterization by proteomics of normal and tumor extracellular matrices. *Mol Cell Proteomics*. 2012;11(4). doi:10.1074/mcp.M111.014647

49. Keane TJ, Londono R, Carey RM, et al. Preparation and characterization of a biologic scaffold from esophageal mucosa. *Biomaterials*. 2013;34(28):6729-6737. doi:10.1016/j.biomaterials.2013.05.052

50. Freytes DO, Martin J, Velankar SS, Lee AS, Badylak SF. Preparation and rheological characterization of a gel form of the porcine urinary bladder matrix. *Biomaterials*. 2008;29(11):1630-1637. doi:10.1016/j.biomaterials.2007.12.014

51. Ahlfors J-EW, Billiar KL. Biomechanical and biochemical characteristics of a human fibroblast-produced and remodeled matrix. *Biomaterials*. 2007;28:2183-2191. doi:10.1016/j.biomaterials.2006.12.030

52. Fernández-Pérez J, Ahearne M. The impact of decellularization methods on extracellular matrix derived hydrogels. *Sci Rep*. 2019;9(1):1-12. doi:10.1038/s41598-019-49575-2

53. Sensi F, D'Angelo E, Piccoli M, et al. Recellularized Colorectal Cancer Patient-Derived Scaffolds as In Vitro Pre-Clinical 3D Model for Drug Screening. *Cancers (Basel)*. 2020;12(3):681. doi:10.3390/cancers12030681

54. Landberg G, Fitzpatrick P, Isakson P, et al. Patient-derived scaffolds uncover breast cancer promoting properties of the microenvironment. *Biomaterials*. 2020;235:119705. doi:10.1016/j.biomaterials.2019.119705

55. Zambon JP, Ko IK, Abolbashari M, et al. Comparative analysis of two porcine kidney decellularization methods for maintenance of functional vascular architectures. *Acta Biomater*. 2018;75:226-234. doi:10.1016/j.actbio.2018.06.004

56. Perea-Gil I, Uriarte JJ, Prat-Vidal C, et al. In vitro comparative study of two decellularization protocols in search of an optimal myocardial scaffold for recellularization. *Am J Transl Res*. 2015;7(3):558-573. Accessed December 26, 2020. /pmc/articles/PMC4448195/?report=abstract

57. Ketchedjian A, Jones AL, Krueger P, et al. Recellularization of decellularized allograft scaffolds in ovine great vessel reconstructions. *Ann Thorac Surg*. 2005;79(3):888-896. doi:10.1016/j.athoracsur.2004.09.033

58. Romero-López M, Trinh AL, Sobrino A, et al. Recapitulating the human tumor microenvironment: Colon tumor-derived extracellular matrix promotes angiogenesis and tumor cell growth. *Biomaterials*. 2017;116:118-129. doi:10.1016/j.biomaterials.2016.11.034

59. Cazzaniga W, Nebuloni M, Longhi E, et al. Human Prostate Tissue-derived Extracellular Matrix as a Model of Prostate Microenvironment. *Eur Urol Focus*. 2016;2(4):400-408. doi:10.1016/j.euf.2016.02.016

60. Alfano M, Nebuloni M, Allevi R, et al. Linearized texture of three-dimensional extracellular matrix is mandatory for bladder cancer cell invasion. *Sci Rep*. 2016;6(1):1-12. doi:10.1038/srep36128

61. Barkestani MN, Naserian S, Uzan G, Shamdani S. Post-decellularization techniques ameliorate cartilage decellularization process for tissue engineering applications: *https://doi.org/101177/2041731420983562*. 2021;12. doi:10.1177/2041731420983562

62. Scarritt ME, Pashos NC, Bunnell BA. A Review of Cellularization Strategies for Tissue

Engineering of Whole Organs. *Front Bioeng Biotechnol*. 2015;0(MAR):43. doi:10.3389/FBIOE.2015.00043

63. Saldin LT, Cramer MC, Velankar SS, White LJ, Badylak SF. Extracellular matrix hydrogels from decellularized tissues: Structure and function. *Acta Biomater*. 2017;49:1-15. doi:10.1016/j.actbio.2016.11.068

64. Gordon-Weeks A, Yuzhalin AE. Cancer Extracellular Matrix Proteins Regulate Tumour Immunity. *Cancers (Basel)*. 2020;12(11):1-25. doi:10.3390/CANCERS12113331

65. Müller I, Kulms D. A 3D Organotypic Melanoma Spheroid Skin Model. *J Vis Exp*. 2018;2018(135):57500. doi:10.3791/57500

66. Kenny PA, Lee GY, Myers CA, et al. The morphologies of breast cancer cell lines in three-dimensional assays correlate with their profiles of gene expression. *Mol Oncol*. 2007;1(1):84. doi:10.1016/J.MOLONC.2007.02.004

67. Euhus DM, Hudd C, Laregina MC, Johnson FE. Tumor measurement in the nude mouse. *J Surg Oncol*. 1986;31(4):229-234. doi:10.1002/jso.2930310402

68. Bioconductor - NOISeq. Accessed November 22, 2021. https://bioconductor.org/packages/release/bioc/html/NOISeq.html

69. Feng J, Meyer CA, Wang Q, Liu JS, Liu XS, Zhang Y. GFOLD: a generalized fold change for ranking differentially expressed genes from RNA-seq data. *Bioinformatics*. 2012;28(21):2782-2788. doi:10.1093/BIOINFORMATICS/BTS515

70. Park SY, Lee DG, Jo A, et al. Extracellular Microenvironmental Change by B16F10 Melanoma-derived Proteins Induces Cancer Stem-like Cell Properties from NIH3T3 Cells. *Sci Rep*. 2019;9(1):1-10. doi:10.1038/s41598-019-53326-8

71. Chen P, Cescon M, Bonaldo P. Collagen VI in cancer and its biological mechanisms. *Trends Mol Med*. 2013;19(7):410-417. doi:10.1016/j.molmed.2013.04.001

72. You WK, Bonaldo P, Stallcup WB. Collagen VI ablation retards brain tumor progression due to deficits in assembly of the vascular basal lamina. *Am J Pathol*. 2012;180(3):1145-1158. doi:10.1016/j.ajpath.2011.11.006

73. Hofmann A, Ritz U, Verrier S, et al. The effect of human osteoblasts on proliferation and neo-vessel formation of human umbilical vein endothelial cells in a long-term 3D co-culture on polyurethane scaffolds. *Biomaterials*. 2008;29(31):4217-4226. doi:10.1016/j.biomaterials.2008.07.024